

Carboxylate-Bridged Diiron(II) Complexes: Synthesis, Characterization, and O₂-Reactivity of Models for the Reduced Diiron Centers in Methane Monooxygenase and Ribonucleotide Reductase

Susanna Herold and Stephen J. Lippard*

Contribution from the Department of Chemistry, Massachusetts Institute of Technology, Cambridge, Massachusetts 02139

Received August 14, 1996[⊗]

Abstract: Diiron(II) complexes with an oxygen-rich coordination environment were assembled with the dinucleating dicarboxylate ligands *m*-xylylenediamine bis(Kemp's triacid)imide (H₂XDK) and the more soluble analogue *m*-xylylenediamine bis(propyl Kemp's triacid)imide (H₂PXDK). X-ray crystallographic analysis revealed that, in most of the complexes, only one monodentate N-donor ligand is bound to each iron(II) ion. In addition to XDK and PXDK, a variety of other ligands bridge the dimetallic core including chloride, fluoride, triflate, or carboxylate. The tris(carboxylate-bridged) complexes [Fe₂(μ-XDK)(μ-O₂CPh)(ImH)₂(O₂CPh)(MeOH)] (**3**) and [Fe₂(μ-O₂CC(CH₃)₃)(μ-PXDK)(*N*-MeIm)₂(O₂CC(CH₃)₃)] (**4**) have the same ligand composition as the diiron(II) cores in the hydroxylase component of methane monooxygenase (MMO) and in the R2 protein of ribonucleotide reductase (RNR). The coordination environments of the two iron centers in **3** and **4** are inequivalent, with one iron being 6-coordinate and the other being 4-coordinate. The bridging benzoate and pivalate ligands have an unusual coordination mode with a Fe–O–C bond angle close to 180°. Fits of magnetic susceptibility data collected for several of the complexes between 300 and 4 K indicated that the two iron(II) centers are weakly antiferromagnetically coupled with a coupling constant which does not depend on the nature of the bridging ligands. Mössbauer spectra of polycrystalline and frozen THF solution samples of **4** exhibited two overlapping doublets of equal intensity, reflecting the different coordination environments of the two iron(II) ions. The nearly identical Mössbauer parameters for the solid and frozen solution samples indicate that the dinuclear core remains intact upon dissolution. Stopped-flow studies of the reaction of **3** and **4** with O₂ in THF showed the rapid formation ($k_p \approx 74 \text{ s}^{-1}$ for **3** at 202.5 K and $k_p \approx 300 \text{ s}^{-1}$ for **4** at 197 K) of colored intermediates with broad absorption maxima near 660 and 670 nm, respectively. These values are characteristic of peroxo-to-iron charge-transfer bands and similar to that observed for the (μ-peroxo)-diiron(III) intermediate (H_{peroxo}) in the MMO reaction cycle.

Introduction

Carboxylate-bridged diiron centers occur in the active sites of several proteins involved in reversible dioxygen binding or activation.^{1,2} Significant examples include hemerythrin (Hr),^{3,4} the R2 subunit of ribonucleotide reductase (RNR) from *E. coli*,^{5,6} the hydroxylase component (H) of soluble methane monooxygenase (MMO),^{7,8} rubrerythrin (Rr),^{9,10} stearylacyl carrier protein Δ⁹ desaturase,¹¹ and the ferroxidase center of ferritin.¹² Over the past few years, studies carried out on both proteins

and diiron model complexes have elucidated the geometry and physical properties of the diiron cores at the active sites of these proteins. A focus of current interest is to identify the structural and electronic features responsible for the different mechanisms by which these similar diiron(II) centers react with dioxygen.

Hemerythrin is the only protein of this class which does not activate dioxygen but, instead, binds it reversibly. The X-ray structure of reduced Hr revealed two irons bridged by the carboxylate groups of glutamate and aspartate residues and by a hydroxide ion.^{3,4} The terminal coordination sites are occupied by five histidines, leaving one site available for dioxygen binding. In all other proteins of the class, the coordination spheres of the diiron core are mostly filled with oxygen-donor ligands and have either open sites or weakly coordinated water molecules, which favors interaction with dioxygen. The involvement of iron(II) centers in the reduced enzymes facilitates a four-electron reduction of dioxygen, and the carboxylate-rich ligand environment renders accessible high-valent iron species which may be required for the activation process.¹³

Mechanistic studies of the RNR and MMO systems have identified intermediates involved in the activation of dioxygen. In ribonucleotide reductase, the enzyme which catalyzes the reduction of nucleotides to deoxynucleotides in the first committed step of DNA biosynthesis, a diiron(II) center in the R2 subunit reacts with dioxygen to generate a stable, functionally

[⊗] Abstract published in *Advance ACS Abstracts*, December 15, 1996.

(1) Feig, A. L.; Lippard, S. J. *Chem. Rev.* **1994**, *94*, 759–805.

(2) Nordlund, P.; Eklund, H. *Curr. Opin. Struct. Biol.* **1995**, *5*, 758–766.

(3) Holmes, M. A.; Le Trong, I.; Turley, S.; Sieker, L. C.; Stenkamp, R. E. *J. Mol. Biol.* **1991**, *218*, 583–593.

(4) Holmes, M. A.; Stenkamp, R. E. *J. Mol. Biol.* **1991**, *220*, 723–737.

(5) Nordlund, P.; Eklund, H. *J. Mol. Biol.* **1993**, *232*, 123–164.

(6) Logan, D. T.; Su, X.-D.; Åberg, A.; Regnström, K.; Hajdu, J.; Eklund, H.; Nordlund, P. *Structure* **1996**, *4*, 1053–1064.

(7) Rosenzweig, A. C.; Frederick, C. A.; Lippard, S. J.; Nordlund, P. *Nature* **1993**, *366*, 537–543.

(8) Rosenzweig, A. C.; Nordlund, P.; Takahara, P. M.; Frederick, C. A.; Lippard, S. J. *Chem. Biol.* **1995**, *2*, 409–418.

(9) Gupta, N.; Bonomi, F.; Kurtz, D. M., Jr.; Ravi, N.; Wang, D. L.; Huynh, B. H. *Biochemistry* **1995**, *34*, 3310–3318.

(10) deMaré, F.; Kurtz, D. M., Jr.; Nordlund, P. *Nature Struct. Biol.* **1996**, *3*, 539–546.

(11) Fox, B. G.; Shanklin, J.; Ai, J.; Loehr, T. M.; Sanders-Loehr, J. *Biochemistry* **1994**, *33*, 12776–12786.

(12) Harrison, P. M.; Arosio, P. *Biochim. Biophys. Acta* **1996**, *1275*, 161–203.

(13) Rosenzweig, A. C.; Feng, X.; Lippard, S. J. *Applications of Enzyme Biotechnology*; Plenum Press: New York, 1991; pp 69–85.

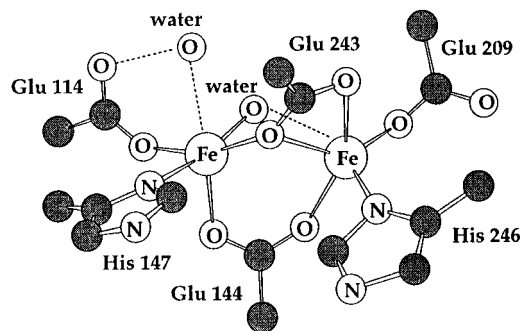


Figure 1. Active site structure of the diiron(II) core in the reduced form of MMOH.

essential tyrosyl radical. X-ray crystallographic studies of reduced R2 revealed the two iron atoms bridged by two carboxylate groups, each being further coordinated by a bidentate carboxylate and a histidine.⁶ Spectroscopic studies of reduced R2 with dioxygen identified an intermediate, designed X, the properties of which have been interpreted with models involving either two high-spin iron(III) ions and a free radical bridging ligand^{14–16} or a mixed-valent bis(μ -oxo)Fe(III)Fe(IV) species.^{17,18} Another incompletely characterized intermediate has been proposed to be a diiron(III) peroxide species.¹⁹ In MMO, the enzyme system which converts methane to methanol in the first metabolic step of methanotrophs, a similar diiron(II) center, located in the hydroxylase component (MMOH), is responsible for dioxygen activation. The two iron(II) ions in MMOH_{red} are bridged by two glutamate carboxylate groups, and the coordination spheres are completed by two additional monodentate glutamate residues and two weakly bound water molecules (Figure 1).⁸ Reaction of MMOH_{red} with dioxygen affords H_{peroxo}, a spectroscopically characterized intermediate.^{20,21} Assignment of this species as a diiron(III) peroxide was facilitated by reference to Mössbauer, optical, and resonance Raman spectroscopic data of (μ -peroxo)diiron(III) model complexes.^{22–24} Three such complexes very recently characterized by X-ray crystallography^{25–27} and two by Mössbauer spectroscopy^{25,27} support the (μ -1,2-peroxo)-coordination mode for H_{peroxo}. A second intermediate, designated Q, has not been

completely characterized but has been tentatively assigned as a high-valent iron(IV) species.^{21,28–30}

Although numerous carboxylate-bridged diiron(III) models with a variety of multidentate nitrogen donor ligands have been synthesized,^{31–36} the focus of current interest is to prepare diiron(II) complexes, in particular, with the goal to obtain functional models for RNR and MMO.^{1,37} Because ligands bound to Fe(II) are kinetically labile, the synthesis of reduced model complexes has been quite challenging. Only a few such complexes are known, most of which have chelating polynitrogen donor ligands and are coordinatively saturated.^{38–46} Reaction of most of these complexes with dioxygen resulted in irreversible oxidation without the formation of any detectable intermediates. In a few cases, stable or metastable (μ -peroxo)diiron(III) intermediates were formed,^{1,22,23,41,45,47} but so far none mimic the chemistry of RNR and MMO, perhaps because the coordination environment of these models differs substantially from that found in the protein active site.

In order to address this deficiency, we have prepared and characterized a variety of diiron(II) complexes with the dinucleating dicarboxylate ligands *m*-xylylenediamine bis(Kemp's triacid)imide, H₂XDK, and the more soluble derivative *m*-xylylenediamine bis(propyl Kemp's triacid)imide, H₂PXDK (Figure 2). As reported in a preliminary communication,⁴⁸ XDK allows for the preparation in good yields of a variety of diiron(II) complexes with different bridging ligands. In this paper we describe in detail the synthesis, X-ray crystal structure determination, Mössbauer spectra, and magnetic properties of some of these and additional complexes. We also report preliminary kinetic studies of the reaction of [Fe₂(μ -XDK)(μ -O₂CPh)(ImH)₂(O₂CPh)(MeOH)] (**3**) and [Fe₂(μ -O₂CC(CH₃)₃)(μ -PXDK)(*N*-MeIm)₂(O₂CC(CH₃)₃)] (**4**) with dioxygen at low temperature. These compounds, which represent good models for the reduced forms of RNR and MMOH, form metastable intermediates with absorption features in the UV-vis spectra

(14) Ravi, N.; Bollinger, J. M., Jr.; Huynh, B. H.; Edmondson, D. E.; Stubbe, J. *J. Am. Chem. Soc.* **1994**, *116*, 8007–8014.

(15) Bollinger, J. M., Jr.; Tong, W. H.; Ravi, N.; Huynh, B. H.; Edmondson, D. E.; Stubbe, J. *J. Am. Chem. Soc.* **1994**, *116*, 8015–8023.

(16) Bollinger, J. M., Jr.; Tong, W. H.; Ravi, N.; Huynh, B. H.; Edmondson, D. E.; Stubbe, J. *J. Am. Chem. Soc.* **1994**, *116*, 8024–8032.

(17) Sturgeon, B. E.; Burdi, D.; Chen, S.; Huynh, B.-H.; Edmondson, D. E.; Stubbe, J.; Hoffman, B. M. *J. Am. Chem. Soc.* **1996**, *118*, 7551–7557.

(18) Burdi, D.; Sturgeon, B. E.; Tong, W. H.; Stubbe, J.; Hoffman, B. M. *J. Am. Chem. Soc.* **1996**, *118*, 281–282.

(19) Tong, W. H.; Chen, S.; Lloyd, S. G.; Edmondson, D. E.; Huynh, B. H.; Stubbe, J. *J. Am. Chem. Soc.* **1996**, *118*, 2107–2108.

(20) Liu, K. E.; Valentine, A. M.; Qiu, D.; Edmondson, D. E.; Appelman, E. H.; Spiro, T. G.; Lippard, S. J. *J. Am. Chem. Soc.* **1995**, *117*, 4997–4998.

(21) Liu, K. E.; Valentine, A. M.; Wang, D.; Huynh, B. H.; Edmondson, D. E.; Salifoglou, A.; Lippard, S. J. *J. Am. Chem. Soc.* **1995**, *117*, 10174–10185.

(22) Brennan, B. A.; Chen, Q.; Juarez-Garcia, C.; True, A. E.; O'Connor, C. J.; Que, L., Jr. *Inorg. Chem.* **1991**, *30*, 1937–1943.

(23) Ménage, S.; Brennan, B. A.; Juarez-Garcia, C.; Münck, E.; Que, L., Jr. *J. Am. Chem. Soc.* **1990**, *112*, 6423–6425.

(24) Micklitz, W.; Bott, S. G.; Bentsen, J. G.; Lippard, S. J. *J. Am. Chem. Soc.* **1989**, *111*, 372–374.

(25) Ookubo, T.; Sugimoto, H.; Nagayama, T.; Masuda, H.; Sato, T.; Tanaka, K.; Maeda, Y.; Okawa, H.; Hayashi, Y.; Uehara, A.; Suzuki, M. *J. Am. Chem. Soc.* **1996**, *118*, 701–702.

(26) Dong, Y.; Yan, S.; Young, V. G., Jr.; Que, L., Jr. *Angew. Chem., Int. Ed. Engl.* **1996**, *35*, 618–620.

(27) Kim, K.; Lippard, S. J. *J. Am. Chem. Soc.* **1996**, *118*, 4914–4915.

(28) Lee, S.-K.; Fox, B. G.; Froland, W. A.; Lipscomb, J. D.; Münck, E. *J. Am. Chem. Soc.* **1993**, *115*, 6450–6451.

(29) Lee, S.-K.; Nesheim, J. C.; Lipscomb, J. D. *J. Biol. Chem.* **1993**, *268*, 21569–21577.

(30) Lipscomb, J. D. *Annu. Rev. Microbiol.* **1994**, *48*, 371–399.

(31) Lippard, S. J. *Angew. Chem., Int. Ed. Engl.* **1988**, *27*, 344–361.

(32) Sanders-Loehr, J. In *Iron Carriers and Iron Proteins*; Loehr, T. M., Ed.; VCH Press: New York, 1989; pp 373–466.

(33) Vincent, J. B.; Olivier-Lilley, G. L.; Averill, B. A. *Chem. Rev.* **1990**, *90*, 1447–1467.

(34) Kurtz, D. M., Jr. *Chem. Rev.* **1990**, *90*, 585–606.

(35) Que, L., Jr.; True, A. E. *Prog. Inorg. Chem.* **1990**, *38*, 97–200.

(36) Que, L., Jr. In *Bioinorganic Catalysis*; Reedijk, J., Ed.; Dekker: New York, 1993; pp 347–393.

(37) Que, L., Jr.; Dong, Y. *Acc. Chem. Res.* **1996**, *29*, 190–196.

(38) Hartman, J. R.; Rardin, R. L.; Chaudhuri, P.; Pohl, K.; Wiegardt, K.; Nuber, B.; Weiss, J.; Papaefthymiou, G. C.; Frankel, R. B.; Lippard, S. J. *J. Am. Chem. Soc.* **1987**, *109*, 7387–7396.

(39) Tolman, W. B.; Liu, S.; Bentsen, J. G.; Lippard, S. J. *J. Am. Chem. Soc.* **1991**, *113*, 152–164.

(40) Stassinopoulos, A.; Schulte, G.; Papaefthymiou, G. C.; Caradonna, J. P. *J. Am. Chem. Soc.* **1991**, *113*, 8686–8697.

(41) Kitajima, N.; Tamura, N.; Tanaka, M.; Moro-oka, Y. *Inorg. Chem.* **1992**, *31*, 3342–3343.

(42) Ménage, S.; Zang, Y.; Hendrich, M. P.; Que, L., Jr. *J. Am. Chem. Soc.* **1992**, *114*, 7786–7792.

(43) Hayashi, Y.; Suzuki, M.; Uehara, A.; Mizutani, Y.; Kitagawa, T. *Chem. Lett.* **1992**, 91–94.

(44) Hagen, K. S.; Lachicotte, R. *J. Am. Chem. Soc.* **1992**, *114*, 8741–8742.

(45) Dong, Y.; Ménage, S.; Brennan, B. A.; Elgren, T. E.; Jang, H. G.; Pearce, L. L.; Que, L., Jr. *J. Am. Chem. Soc.* **1993**, *115*, 1851–1859.

(46) Coucouvanis, D.; Reynolds, R. A., III; Dunham, W. R. *J. Am. Chem. Soc.* **1995**, *117*, 7570–7571.

(47) Hayashi, Y.; Kayatani, T.; Sugimoto, H.; Suzuki, M.; Inomata, K.; Uehara, A.; Mizutani, Y.; Kitagawa, T.; Maeda, Y. *J. Am. Chem. Soc.* **1995**, *117*, 11220–11229.

(48) Herold, S.; Pence, L. E.; Lippard, S. J. *J. Am. Chem. Soc.* **1995**, *117*, 6134–6135.

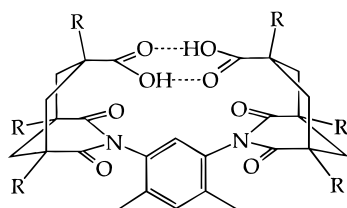
H₂XDK, R = CH₃H₂PXDK, R = (CH₂)₂CH₃

Figure 2. Schematic representation of the bis(carboxylate) ligands H₂XDK and H₂PXDK.

characteristic of peroxide-to-iron charge-transfer bands of (μ -peroxo)diiron(III) species and similar to those obtained for the H_{peroxo} intermediate in the reaction cycle of MMO. Reactions of the other diiron(II) complexes, which have chloride, fluoride, or triflate, as well as XDK, bridging ligands not present in the proteins, did not show any such intermediate during their reactions with dioxygen.

Experimental Section

General Procedures and Methods. Solvents were dried and distilled under nitrogen by standard procedures. Unless otherwise noted, reagents were obtained from commercial suppliers and used as received. The ligand H₂XDK was prepared according to a literature procedure.^{49–51} All manipulations and reactions were carried out under an inert atmosphere in a Vacuum Atmospheres glovebox or by using standard Schlenk techniques. FTIR spectra in the range 4000–400 cm⁻¹ were obtained and manipulated by using a Bio-Rad SPC3200 FTIR instrument. UV–vis spectra were recorded with a Hewlett-Packard 8452 diode array spectrophotometer. Spectra of metastable dioxygen adducts were collected at low temperature with a specially modified Dewar flask with quartz windows. ¹H NMR spectra were obtained on a Bruker AC-250 spectrometer.

Synthetic Procedures. *cis,cis*-1,3,5-Tripropylcyclohexyl 1,3,5-Anhydride Acid Chloride (1). The triacid *cis,cis*-1,3,5-tripropylcyclohexane-1,3,5-tricarboxylic acid⁵² (45 g, 131 mmol) was allowed to react with an excess of thionyl chloride (180 mL, 2.4 mol) by following the procedure described for the synthesis of the analogous trimethyl derivative,^{50,51} yielding 40 g (90%) of the acid chloride **1** as a white solid. ¹H NMR (250 MHz, CDCl₃): δ 2.72 (2H, d, *J* = 14.5 Hz), 2.11 (1H, d, *J* = 13.5 Hz), 1.95 (2H, m), 1.60 (2H, m), 1.49–1.17 (11H, m), 0.96–0.86 (9H, m).

***m*-Xylylenediamine Bis(propyl Kemp's triacidimide), H₂PXDK (2).** The acid chloride **1** (28.3 g, 81.9 mmol) was allowed to react with 1,3-dimethyl-4,6-diaminobenzene (5.58 g, 40.95 mmol) and 4-(dimethylamino)pyridine (150 mg, 0.123 mmol) in dry pyridine (~250 mL) by following the procedure described for the synthesis of H₂XDK.^{49,51} Recrystallization from hot MeOH or MeOH/Et₂O yielded **2** as a pale tan solid (20 g, 65%). ¹H NMR (250 MHz, CDCl₃): δ 7.09 (1H, s), 6.62 (1H, s), 2.70 (4H, d, *J* = 13.8 Hz), 2.37 (2H, d, *J* = 13.0 Hz), 2.05–1.92 (10H, m), 1.52–1.19 (26H, m), 0.92–0.82 (18H, m). FTIR (KBr, cm⁻¹): 2961, 2934, 2874, 1734, 1706, 1685, 1509, 1465, 1457, 1437, 1405, 1374, 1327, 1314, 1248, 1184, 1118, 1108, 1054, 1034, 996, 921, 862, 782, 762, 737, 588, 538, 461, 450, 419. Anal. Calcd for **2**, C₄₄H₆₄N₂O₈: C, 70.56; H, 8.61; N, 3.74. Found: C, 70.91; H, 8.67; N, 3.89.

[Fe₂(μ -O₂CPh)(μ -XDK)(ImH)₂(O₂CPh)(MeOH)]·0.5MeOH·H₂O (3·0.5MeOH·H₂O). A solution of [Fe(H₂O)₆](BF₄)₂ (258 mg, 0.76 mmol) in MeOH (5 mL) was added to a solution of H₂XDK

(222 mg, 0.38 mmol) and Et₃N (77 mg, 0.76 mmol) in CH₂Cl₂ (5 mL). Addition of solutions of imidazole (52 mg, 0.76 mmol) in CH₂Cl₂ (5 mL) and (Me₄N)(O₂CPh) (222 mg, 1.14 mmol) in MeOH (5 mL) yielded a deep yellow reaction mixture, which was stirred at room temperature for 2 h. The precipitated BF₄⁻ salts were filtered, and the resulting filtrate was evaporated to dryness. The deep yellow residue was dissolved in a mixture of MeOH/CH₂Cl₂ (2:1, ca. 2–3 mL), filtered again if required, and layered with Et₂O (~15 mL). After a few days, deep yellow X-ray quality crystals of [Fe₂(μ -O₂CPh)(μ -XDK)(ImH)₂(O₂CPh)(MeOH)]·0.5MeOH·H₂O (**3·0.5MeOH·H₂O**) were collected, washed with CH₂Cl₂ and Et₂O, and dried (280 mg, 66%). To separate small amounts of [Fe(HXDK)₂(MeOH)₂], which sometimes coprecipitated with **3**, the obtained solid was stirred in CH₂Cl₂ for 1 h. The complex [Fe(HXDK)₂(MeOH)₂] remained in solution whereas the pale yellow powder of **3** was filtered and washed with Et₂O. FTIR (KBr, cm⁻¹): 3304, 3139, 3062, 2966, 2933, 2900, 1729, 1685, 1608, 1536, 1494, 1460, 1414, 1381, 1334, 1281, 1264, 1248, 1228, 1194, 1185, 1138, 1087, 1070, 1026, 985, 958, 950, 943, 893, 851, 762, 715, 685, 660, 613, 473, 463, 449, 431. Anal. Calcd for **3**·H₂O, C₅₃H₆₂N₆O₁₄·Fe₂: C, 56.90; H, 5.59; N, 7.51. Found: C, 56.77; H, 5.42; N, 7.90.

[Fe₂(μ -O₂CC(CH₃)₃)(μ -PXDK)(*N*-MeIm)₂(O₂CC(CH₃)₃)]·C₅H₁₂ (4·C₅H₁₂). To a solution of [Fe(H₂O)₆](BF₄)₂ (402 mg, 1.2 mmol) in MeOH (2 mL) were added the following solutions in the given order: H₂PXDK (450 mg, 0.6 mmol) and Et₃N (120 mg, 1.2 mmol) in CH₂Cl₂ (10 mL), *N*-methylimidazole (99 mg, 1.2 mmol) in CH₂Cl₂ (10 mL), and (Me₄N)(O₂CC(CH₃)₃) (315 mg, 1.8 mmol) in MeOH (3 mL). The reaction mixture was stirred for 2 h at room temperature, then the precipitated BF₄⁻ salts were filtered, and the resulting pale brown solution was evaporated to dryness. The residue was dissolved in ~4 mL of CH₂Cl₂, filtered again, and layered with pentane (~15 mL). After ca. 15 h the precipitated off-white crystals, characterized by FTIR as a mixture of predominantly BF₄⁻ salts, were separated. Pentane (~15 mL) was added to the remaining solution, and the complex [Fe₂(μ -O₂CC(CH₃)₃)(μ -PXDK)(*N*-MeIm)₂(O₂CC(CH₃)₃)]·C₅H₁₂ (**4·C₅H₁₂**) was crystallized by slow evaporation of the solvents. The obtained pale yellow X-ray quality crystals (470 mg, 60%) were washed with pentane. FTIR (KBr, cm⁻¹): 2960, 2929, 2874, 1734, 1690, 1604, 1539, 1485, 1457, 1437, 1423, 1361, 1245, 1227, 1189, 1109, 1090, 1028, 925, 896, 861, 793, 762, 739, 659, 615, 609, 540, 434. Anal. Calcd for **4**·C₅H₁₂, C₆₇H₁₀₄N₆O₁₂Fe₂: C, 62.03; H, 8.08; N, 6.48. Found: C, 61.80; H, 7.95; N, 6.26.

[Fe₂(μ -F)(μ -XDK)(*N*-MeIm)₂(MeOH)_{2.5}(H₂O)_{0.5}](BF₄)·MeOH (5·MeOH). A solution of [Fe(H₂O)₆](BF₄)₂ (67 mg, 0.2 mmol), H₂XDK (58 mg, 0.1 mmol), Et₃N (20 mg, 0.2 mmol), distilled *N*-methylimidazole (16 mg, 0.2 mmol), and Et₃N (20 mg, 0.2 mmol) or Me₄NOH·5H₂O (36 mg, 0.2 mmol) in 10 mL of CH₂Cl₂/MeOH (1:1) was stirred for 2 h. The reaction mixture was filtered, concentrated to 4–5 mL, filtered again if required, and layered with Et₂O (~15 mL). The resulting almost colorless X-ray quality crystals of [Fe₂(μ -F)(μ -XDK)(*N*-MeIm)₂(MeOH)_{2.5}(H₂O)_{0.5}](BF₄)·MeOH (**5·MeOH**) were collected, washed with MeOH and Et₂O, and dried under vacuum (yield 60 mg, 57%). It was difficult always to obtain pure material, because BF₄⁻ salts coprecipitated with **5** and were difficult to separate. FTIR (KBr, cm⁻¹): 3411, 3136, 2963, 2930, 1734, 1690, 1636, 1534, 1510, 1461, 1422, 1380, 1360, 1336, 1303, 1289, 1233, 1197, 1094, 1053, 1038, 957, 937, 878, 849, 828, 779, 765, 661, 620, 577, 474, 451. Anal. Calcd for **5**, C_{42.5}H₆₁N₆O₁₁BF₃Fe₂: C, 48.64; H, 5.86; N, 8.01. Found: C, 49.09; H, 6.18; N, 8.16.

[Fe₂(μ -OTf)(μ -XDK)(*N*-MeIm)₃(MeOH)(H₂O)](OTf)·MeOH·CH₂Cl₂ (6·MeOH·CH₂Cl₂). Solutions of [Fe(H₂O)₆](OTf)₂ (92 mg, 0.2 mmol) in MeOH (6 mL), H₂XDK (58 mg, 0.1 mmol) and Et₃N (20 mg, 0.2 mmol) in CH₂Cl₂ (3 mL), and distilled *N*-methylimidazole (25 mg, 0.3 mmol) in CH₂Cl₂ (3 mL) were mixed in the given order and stirred for 2 h at room temperature. A very small amount of a green precipitate was filtered, and the resulting pale yellow solution was concentrated to 2–3 mL, filtered again if required, and layered with Et₂O (~15 mL). The resulting colorless X-ray quality crystals of [Fe₂(μ -OTf)(μ -XDK)(*N*-MeIm)₃(MeOH)(H₂O)](OTf)·MeOH·CH₂Cl₂ (**6·MeOH·CH₂Cl₂**) that deposited were collected, washed with Et₂O, and dried under vacuum (yield 120 mg, 93%). FTIR (KBr, cm⁻¹): 3462, 3133, 2971, 2935, 1718, 1676, 1602, 1535, 1502, 1466, 1427, 1408, 1383, 1364, 1336, 1306, 1277, 1229, 1203, 1185, 1153, 1110,

(49) Watton, S. P.; Masschelein, A.; Rebek, J., Jr.; Lippard, S. J. *J. Am. Chem. Soc.* **1994**, *116*, 5196–5205.

(50) Rebek, J., Jr.; Marshall, L.; Wolak, R.; Parris, K.; Killoran, M.; Askew, B.; Nemeth, D.; Islam, N. *J. Am. Chem. Soc.* **1985**, *107*, 7476–7481.

(51) Marshall, L.; Parris, K.; Rebek, J., Jr.; Luis, S. V.; Burguete, M. I. *J. Am. Chem. Soc.* **1988**, *110*, 5192–5193.

(52) Jeong, K.-S.; Muehldorf, A. V.; Rebek, J., Jr. *J. Am. Chem. Soc.* **1990**, *112*, 6144–6145.

1095, 1031, 984, 962, 952, 944, 888, 854, 829, 764, 662, 637, 621, 572, 518, 478, 453, 427. Anal. Calcd for **6**, $C_{47}H_{62}N_8O_{16}F_6S_2Fe_2$: C, 43.94; H, 4.86; N, 8.72; F, 8.87. Found: C, 43.27; H, 4.85; N, 8.72; F, 9.12.

[Fe₂(μ-Cl)(μ-XDK)(N-MeIm)₂(MeOH)₃](BF₄)·MeOH (7·MeOH). Method A. A solution of H₂XDK (174 mg, 0.3 mmol) and Et₃N (60 mg, 0.6 mmol) in CH₂Cl₂ (3 mL) was added to a solution of [Fe(H₂O)₆](BF₄)₂ (201 mg, 0.6 mmol) in MeOH (3 mL). Subsequent addition of solutions of distilled *N*-methylimidazole (49 mg, 0.6 mmol) in CH₂Cl₂ (3 mL) and Et₄NCl (51 mg, 0.3 mmol) in MeOH (3 mL) yielded a colorless reaction mixture which was stirred for 2 h at room temperature. The reaction mixture was filtered, concentrated to 3–4 mL, filtered again if required, and layered with Et₂O (~30 mL). The resulting pale pink (almost colorless) X-ray quality crystals of [Fe₂(μ-Cl)(μ-XDK)(N-MeIm)₂(MeOH)₃](BF₄)·MeOH (**7·MeOH**) that deposited were collected, washed with MeOH and Et₂O, and dried under vacuum (yield 280 mg, 84%). FTIR (KBr, cm⁻¹): 3447, 3134, 2970, 2931, 1734, 1678, 1617, 1533, 1509, 1462, 1422, 1404, 1380, 1361, 1244, 1196, 1092, 1054, 1037, 957, 937, 849, 827, 765, 661, 616. Anal. Calcd for **7·MeOH**, $C_{44}H_{66}N_8O_{12}BCl_4Fe_2$: C, 47.83; H, 6.02; N, 7.61; Cl, 3.21. Found: C, 47.03; H, 5.69; N, 7.60; Cl, 2.82.

Method B. Solutions of [Fe(H₂O)₆](BF₄)₂ (40 mg, 0.12 mmol), distilled *N*-methylimidazole (13 mg, 0.16 mmol), and Me₄NCl (13 mg, 0.08 mmol) in a total amount of 5 mL of MeOH were added successively to a mixture of [Fe(HXDK)₂(MeOH)₂] (**8**) (51 mg, 0.04 mmol) and Et₃N (12 μL, 0.08 mmol) in CH₂Cl₂ (5 mL) and stirred for 2 h. The pale yellow reaction mixture was filtered, concentrated to 4–5 mL, filtered again if required, and layered with Et₂O (~15 mL). Pale pink crystals of **7** that deposited were collected, washed with MeOH and Et₂O, and dried briefly under vacuum (76 mg, 86%). The material obtained had an FTIR spectrum identical to that isolated by method A.

[Fe(HXDK)₂(MeOH)₂] (8**).** A mixture of H₂XDK (75 mg, 0.13 mmol) and Et₃N (13 mg, 0.13 mmol) in MeOH (3 mL) was added to a solution of [Fe(H₂O)₆](BF₄)₂ (22 mg, 0.065 mmol) in MeOH (3 mL). A white precipitate immediately formed. After 2 h the precipitate was filtered, washed with Et₂O, and dried under vacuum (77 mg, 93%). Crystals of **8** suitable for X-ray diffraction studies were obtained by layering a mixture of [Fe(H₂O)₆](BF₄)₂ (51 mg, 0.15 mmol) and H₂XDK (88 mg, 0.15 mmol) in MeOH (10 mL) with a solution of Et₃N (30 mg, 0.3 mmol) in MeOH (10 mL). FTIR (KBr, cm⁻¹): 2969, 2929, 1733, 1684, 1616, 1510, 1461, 1423, 1404, 1380, 1360, 1195, 1184, 1086, 957, 880, 849, 763, 758, 573, 537, 451. Anal. Calcd for **8**, $C_{66}H_{86}N_4O_{18}Fe$: C, 61.97; H, 6.78; N, 4.38. Found: C, 61.38; H, 6.94; N, 4.33.

Reaction of [Fe₂(μ-Cl)(μ-XDK)(N-MeIm)₂(MeOH)₃](BF₄) (7**) with TiO₂CCH₃. Preparation of [Fe₂(μ-O₂CCH₃)(μ-XDK)(N-MeIm)₂(MeOH)₃](BF₄) (**9**).** A solution of thallium(I) acetate (13 mg, 0.05 mmol) in MeOH (2 mL) was added to a CH₂Cl₂ solution (4 mL) of [Fe₂(μ-Cl)(μ-XDK)(N-MeIm)₂(MeOH)₃](BF₄) (**7**) (55 mg, 0.05 mmol). After the reaction mixture was stirred for 30 min, the precipitated TiCl₄ was filtered off. The resulting solution was reduced to a volume of 3–4 mL, and colorless crystals were obtained by Et₂O vapor diffusion. The X-ray analysis showed the presence of both the dinuclear complex [Fe₂(μ-O₂CCH₃)(μ-XDK)(N-MeIm)₂(MeOH)₃](BF₄) (**9**) and the mononuclear complex [Fe(HXDK)₂(MeOH)₂] (**8**). FTIR (KBr, cm⁻¹) (mixture of **8** and **9**): 3410, 2981, 2928, 1739, 1671, 1622, 1538, 1464, 1411, 1380, 1364, 1336, 1315, 1230, 1196, 1099, 1067, 1012, 959, 853, 766, 661, 621, 520, 440.

X-ray Crystallography. General Procedures. X-ray diffraction studies of **3** and **5–9** were performed with an Enraf-Nonius CAD-4F Kappa geometry diffractometer and graphite-monochromatized Mo Kα radiation ($\lambda = 0.71069 \text{ \AA}$) by using methods described previously.⁵³ The crystal temperature was maintained by the use of an Enraf-Nonius FR558-S liquid nitrogen cryostat. No appreciable decay was observed for the six compounds, as judged by periodic monitoring of the intensities of three standard reflections. A systematic search for the highest possible Laue symmetry was conducted by using TRACER.⁵⁴

(53) Carnahan, E. M.; Rardin, R. L.; Bott, S. G.; Lippard, S. J. *Inorg. Chem.* **1992**, *31*, 5193–5201.

(54) Lawton, S. L. *TRACER II: A Fortran Lattice Transformation-Cell Reduction Program*; Mobil Oil Corp.: Paulsboro, NJ, 1967.

Initial iron atomic coordinates were obtained by using the direct method program SHELXS-86.⁵⁵ The remaining heavy atoms were located with DIRDIF phase refinements and difference Fourier maps.⁵⁶ Absorption corrections based on ψ scans were applied for **5**, **6**, **8**, and **9**,⁵⁷ and an empirical absorption correction (DIFABS)⁵⁸ was applied for **3**. All calculations for **3** and **6–9** were performed with a VAXstation 4000-90 computer and the TEXSAN software package.⁵⁹ The refinement of **5** was carried out with the SHELXTL software package.⁶⁰ Hydrogen atoms were placed at calculated positions ($C-H = 0.95 \text{ \AA}$), with hydrogen thermal parameters set equal to $1.2B_{eq}$ of the atom to which they were bound. They were included, but not refined, in the final least-squares cycles.

X-ray diffraction studies of **4** were carried out on a Siemens CCD X-ray diffraction system with graphite-monochromatized Mo Kα radiation ($\lambda = 0.71073 \text{ \AA}$) controlled by a pentium-based PC running the SMART software package,⁶¹ as previously described.⁶² The crystal temperature was maintained at 193 K with a Siemens LT-2A nitrogen cryostat. No appreciable decay was observed for the complex, as judged by recollecting, at the end of data acquisition, the initial 50 frames of the first data shell. The raw data frames were integrated by the SAINT software package⁶³ on a Silicon Graphics Indy workstation. The structure of **4** was solved by direct methods by using SIR-92⁶⁴ and was refined by full matrix least-squares and Fourier techniques with TEXSAN.⁵⁹

Relevant crystallographic data for complexes **3–8** are summarized in Table 1, and selected bond distances and angles for **3–5** and **7** are given in Tables 2 and 3. A full crystallographic report, including complete listings of atomic coordinates and B_{eq} , anisotropic thermal parameters, and intramolecular bond distances and angles is available as Supporting Information (Tables S1–S26) together with complete ORTEP diagrams of **3–7** and **9** (Figures S2–S6 and S8) and the numbering schemes for the XDK and the PXDK ligands (Figures S1 and S7).

[Fe₂(μ-O₂CPh)(μ-XDK)(ImH)₂(O₂CPh)(MeOH)]·0.5MeOH·H₂O (3**).** Data were collected at 199 K with the $\omega-2\theta$ scan technique. The positions of the Fe-, N-, and O-atoms, the carboxylate C-atoms of XDK, and all non-hydrogen atoms of the imidazole and benzoate groups were refined anisotropically. The thermal parameter of the C-atom of the coordinated MeOH molecule is high, $B_{eq} = 13(1)$, so we do not rule out the possibility that this position is half occupied by a water molecule. The largest peak in the final difference Fourier map was $1.2 e^{-}/\text{\AA}^3$, located in the vicinity of the MeOH molecule in the lattice.

[Fe₂(μ-F)(μ-XDK)(N-MeIm)₂(MeOH)_{2.5}(H₂O)_{0.5}](BF₄)·MeOH (5**).** Data were collected at 213 K with the $\omega-2\theta$ scan technique. The negative intensity data and 15 severe outlying reflections were omitted from the refinement. The positions of all non-hydrogen atoms were refined anisotropically, except for those of the disordered BF₄⁻ counterion, the C-atom of one of the coordinated MeOH, C(2), the disordered O-atom of a second coordinated MeOH, and the lattice MeOH molecule, which were refined with isotropic temperature factors. The previously communicated structure⁴⁸ was rerefined with an improved model for the disordered atoms. One MeOH molecule coordinated to Fe(1) was disordered over two different positions and modeled with two O-atoms, O(1) and O(1a), refined at half occupancy and bound to the same fully occupied C-atom, C(1). This solution

(55) Sheldrick, G. M. *SHELX86. Program for crystal structure determination*; University of Göttingen: Göttingen, Germany, 1986.

(56) Parthasarathi, V.; Beurskens, P. T.; Slot, H. J. B. *Acta Crystallogr.* **1983**, *A39*, 860–864.

(57) North, A. C. T.; Phillips, D. C.; Mathews, F. S. *Acta Crystallogr.* **1968**, *A24*, 351–359.

(58) Walker, N.; Stuart, D. *Acta Crystallogr.* **1983**, *A39*, 158–166.

(59) TEXSAN: *Single Crystal Structure Analysis Software*, Version 1.6; Molecular Structure Corp.: The Woodlands, TX, 1993.

(60) Sheldrick, G. M. *Siemens Industrial Automation, Inc.*; Analytical Instrumentation: Madison, WI, 1994.

(61) SMART *Siemens Industrial Automation, Inc.*; Analytical Instrumentation: Madison, WI, 1994.

(62) Feig, A. L.; Bautista, M. T.; Lippard, S. J. *Inorg. Chem.* **1996**, *35*, 6892–6898.

(63) SAINT *Siemens Industrial Automation, Inc.*; Analytical Instrumentation: Madison, WI, 1995.

(64) Burla, M. C.; Camalli, M.; Cascarano, G.; Giacovazzo, C.; Polidori, G.; Spagna, R.; Viterbo, D. *J. Appl. Crystallogr.* **1989**, *22*, 389–393.

Table 1. X-ray Crystallographic Information for $[\text{Fe}_2(\mu\text{-O}_2\text{CPh})(\mu\text{-XDK})(\text{ImH})_2(\text{O}_2\text{CPh})(\text{MeOH})]\cdot 0.5\text{MeOH}\cdot\text{H}_2\text{O}$ (**3**·0.5MeOH·H₂O), $[\text{Fe}_2(\mu\text{-O}_2\text{CC}(\text{CH}_3)_3)(\mu\text{-PXDK})(N\text{-MeIm})_2(\text{O}_2\text{CC}(\text{CH}_3)_3)]\cdot\text{C}_5\text{H}_{12}$ (**4**·C₅H₁₂), $[\text{Fe}_2(\mu\text{-F})(\mu\text{-XDK})(N\text{-MeIm})_2(\text{MeOH})_{2.5}(\text{H}_2\text{O})_{0.5}](\text{BF}_4)\cdot\text{MeOH}$ (**5**·MeOH), $[\text{Fe}_2(\mu\text{-OTf})(\text{XDK})(N\text{-MeIm})_3(\text{MeOH})(\text{H}_2\text{O})](\text{OTf})\cdot\text{MeOH}\cdot\text{CH}_2\text{Cl}_2$ (**6**·MeOH·CH₂Cl₂), $[\text{Fe}_2(\mu\text{-Cl})(\text{XDK})(N\text{-MeIm})_2(\text{MeOH})_3](\text{BF}_4)\cdot\text{MeOH}$ (**7**·MeOH), and $[\text{Fe}(\text{HXDK})_2(\text{MeOH})_2]$ (**8**)

	3 ·0.5MeOH·H ₂ O	4 ·C ₅ H ₁₂	5 ·MeOH	6 ·MeOH·CH ₂ Cl ₂	7 ·MeOH	8
formula	Fe ₂ C _{53.5} H ₆₄ N ₆ O _{14.5}	Fe ₂ C ₆₇ H ₁₁₄ N ₆ O ₁₂	Fe ₂ C _{43.5} H ₆₅ N ₆ O ₁₂ BF ₅	Fe ₂ C ₄₉ H ₆₈ N ₈ O ₁₇ Cl ₂ F ₆ S ₂	Fe ₂ C ₄₄ H ₆₆ N ₆ O ₁₂ BClF ₄	FeC ₆₆ H ₈₆ N ₄ O ₁₈
mol wt (g mol ⁻¹)	1134.83	1307.36	1081.52	1401.83	1104.99	1279.27
cryst system	triclinic	monoclinic	monoclinic	orthorhombic	monoclinic	monoclinic
space group	<i>P</i> $\bar{1}$	<i>P</i> 2 ₁ / <i>n</i>	<i>P</i> 2 ₁ / <i>n</i>	<i>Pbcn</i>	<i>P</i> 2 ₁ / <i>n</i>	<i>P</i> 2 ₁ / <i>n</i>
<i>a</i> (Å)	12.631(2)	16.4202(1)	11.930(2)	22.57(1)	12.054(2)	14.509(4)
<i>b</i> (Å)	16.889(4)	20.2320(3)	22.971(6)	23.165(3)	23.051(4)	14.749(1)
<i>c</i> (Å)	17.640(3)	21.4976(3)	18.817(6)	22.636(4)	18.860(3)	15.591(6)
α (deg)	62.19(2)					
β (deg)	72.58(1)	95.437(1)	92.93(2)		94.24(2)	94.28(4)
γ (deg)	87.42(2)					
<i>V</i> (Å ³)	3156(1)	7109.6(1)	5150(2)	11835(4)	5226(2)	3327(2)
<i>Z</i>	2	4	4	8	4	4
ρ_{calc} (g cm ⁻³)	1.19	1.22	1.39	1.59	1.40	1.28
total no. of data	10693	26881	10083	11604	8468	5908
no. of unique data ^{a,b}	3280 ^a	3339 ^a	6729 ^b	4347 ^a	4350 ^a	3462 ^a
no. of parameters	518	465	611	658	404	421
<i>R</i> ^c	0.080	0.075	0.078	0.092	0.069	0.045
<i>R</i> _w ^{d,e}	0.117 ^d	0.083 ^d	0.226 ^e	0.118 ^d	0.095 ^d	0.053 ^d
largest shift/esd, final	0.000	0.003	0.009	0.005	0.000	0.000

^a Observation criterion $I > 3\sigma(I)$. ^b Observation criterion $I > 2\sigma(I)$. ^c $R = \sum(|F_o| - |F_c|)/\sum|F_o|$. ^d $R_w = [\sum_w(|F_o| - |F_c|)^2/\sum_w|F_o|^2]^{1/2}$, where $w = 1/\sigma^2(F)$ and σ is defined in ref 53. ^e $wR2 = \{[\sum[w(F_o^2 - F_c^2)^2]/\sum[w(F_o^2)^2]]^{1/2}$, where $w = 1/[\sigma^2(F_o^2) + 0.1571(P)^2 + 12.43(P)]$ and $P = [\max(0, F_o^2) + 2F_c^2]/3$.

Table 2. Selected Bond Lengths (Å) and Angles (deg) for $[\text{Fe}_2(\mu\text{-XDK})(\mu\text{-O}_2\text{CPh})(\text{ImH})_2(\text{O}_2\text{CPh})(\text{MeOH})]\cdot 0.5\text{MeOH}\cdot\text{H}_2\text{O}$ (**3**·0.5MeOH·H₂O) and $[\text{Fe}_2(\mu\text{-O}_2\text{CC}(\text{CH}_3)_3)(\mu\text{-PXDK})(N\text{-MeIm})_2(\text{O}_2\text{CC}(\text{CH}_3)_3)]\cdot\text{C}_5\text{H}_{12}$ (**4**·C₅H₁₂)^a

Bond Lengths					
	3	4	3	4	4
Fe(1)···Fe(2)	3.609(4)	3.584(3)	Fe(2)–O(13)	2.04(2)	2.048(8)
Fe(1)–O(X) ^b	2.12(1)	2.228(9)	Fe(2)–O(102)	1.97(1)	1.983(9)
Fe(1)–O(10)	2.10(2)	2.144(8)	Fe(2)–O(202)	1.98(1)	2.020(9)
Fe(1)–O(12)	2.20(1)	2.186(9)	Fe(2)–N(3)	2.05(2)	2.07(1)
Fe(1)–O(101)	2.06(1)	2.109(9)			
Fe(1)–O(201)	2.15(1)	2.065(8)	Fe(2)···O(12)	2.52(2)	2.466(8)
Fe(1)–N(1)	2.13(1)	2.16(1)	O(1)···O(11)	2.50(2)	

Bond Angles					
	3	4	3	4	4
O(X)–Fe(1)–O(10) ^b	85.6(5)	60.6(3)	O(12)–Fe(2)–O(13)	56.0(5)	57.4(3)
O(X)–Fe(1)–O(12) ^b	92.3(5)	94.2(3)	O(12)–Fe(2)–O(102)	93.4(5)	89.2(3)
O(X)–Fe(1)–O(101) ^b	177.2(6)	162.9(3)	O(12)–Fe(2)–O(202)	86.4(5)	89.1(3)
O(X)–Fe(1)–O(201) ^b	86.9(5)	97.2(3)	O(12)–Fe(2)–N(3)	162.5(5)	163.2(4)
O(X)–Fe(1)–N(1) ^b	94.4(5)	91.2(4)	O(13)–Fe(2)–O(102)	107.8(6)	107.0(3)
O(10)–Fe(1)–O(12)	90.4(5)	93.0(3)	O(13)–Fe(2)–O(202)	106.5(6)	110.2(3)
O(10)–Fe(1)–O(101)	91.7(5)	102.4(3)	O(13)–Fe(2)–N(3)	107.1(6)	106.0(4)
O(10)–Fe(1)–O(201)	172.5(5)	157.8(4)	O(102)–Fe(2)–O(202)	138.2(5)	134.3(3)
O(10)–Fe(1)–N(1)	89.7(6)	94.7(3)	O(102)–Fe(2)–N(3)	96.4(6)	94.1(4)
O(12)–Fe(1)–O(101)	87.1(5)	89.1(3)	O(202)–Fe(2)–N(3)	95.7(6)	100.2(4)
O(12)–Fe(1)–O(201)	89.6(5)	87.6(3)			
O(12)–Fe(1)–N(1)	173.3(5)	172.0(4)	Fe(1)–O(12)–Fe(2)	99.3(6)	100.6(3)
O(101)–Fe(1)–O(201)	95.8(5)	99.8(3)	Fe(1)–O(12)–C(Y) ^c	178(1)	175.3(9)
O(101)–Fe(1)–N(1)	86.2(5)	87.5(4)	Fe(2)–O(12)–C(Y) ^c	80(1)	79.6(8)
O(201)–Fe(1)–N(1)	91.1(6)	85.9(3)	Fe(2)–O(13)–C(Y) ^c	102(1)	99.1(9)

^a Estimated standard deviations in the last significant figure are given in parentheses. See Figures 3, 4, S1, S2, S7, and S8 for atom-labeling schemes. ^b X = 1 in **3** and 11 in **4**. ^c Y = 18 in **3** and 16 in **4**.

was preferred over a model consisting of only one O-atom because it gave Fe–O distances closer to those found in the isostructural chloride-bridged complex. Initial attempts to refine the C-atom, C(2), of the second MeOH coordinated to Fe(1) at full occupancy resulted in high thermal parameters. The electron density was more satisfactorily accounted for with C(2) refined at half occupancy, indicating that this site is probably half occupied by a H₂O and a MeOH molecule. The BF₄⁻ counterion exhibited 3-fold disorder and was modeled with one F-atom, F(2), refined at full occupancy; the residual electron density was modeled with two sets of three F-atoms, F(3), F(4), F(5) and F(3a),

F(4a), F(5a), each refined at half occupancy. The largest peak in the final difference Fourier map was 0.99 e⁻/Å³, located in the vicinity of C(2).

[Fe₂(μ-OTf)(μ-XDK)(N-MeIm)₃(MeOH)(H₂O)](OTf)·MeOH·CH₂Cl₂ (6·MeOH·CH₂Cl₂). Data were collected at 199 K with the ω–2θ scan technique. The positions of all non-hydrogen atoms were refined anisotropically, except for the disordered atoms of the bridging triflate and the lattice molecules, which were refined with isotropic temperature factors. The bridging triflate exhibits a 2-fold disorder which was modeled with the two coordinated O-atoms, O(10)

Table 3. Selected Bond Lengths (Å) and Angles (deg) for $[\text{Fe}_2(\mu\text{-XDK})(\mu\text{-F})(N\text{-MeIm})_2(\text{MeOH})_3](\text{BF}_4)\cdot\text{MeOH}$ (**5**·**MeOH**) and $[\text{Fe}_2(\mu\text{-XDK})(\mu\text{-Cl})(N\text{-MeIm})_2(\text{MeOH})_3](\text{BF}_4)\cdot\text{MeOH}$ (**7**·**MeOH**)^a

	Bond Lengths				
	5·MeOH	7·MeOH	5·MeOH	7·MeOH	
Fe(1)···Fe(2)	3.397(2)	3.552(2)	Fe(2)–X(1) ^b	2.166(4)	2.462(4)
Fe(1)–X(1) ^b	2.230(5)	2.493(4)	Fe(2)–O(3)	2.233(6)	2.18(1)
Fe(1)–O(1) ^c	2.234(11)	2.21(1)	Fe(2)–O(102)	1.994(6)	2.009(8)
Fe(1)–O(2)	2.246(10)	2.21(2)	Fe(2)–O(202)	1.981(5)	1.99(1)
Fe(1)–O(101)	2.123(7)	2.10(1)	Fe(2)–N(3)	2.089(7)	2.09(1)
Fe(1)–O(201)	2.089(6)	2.061(8)	O(1)···O(103) ^c	3.01(2)	2.97(2)
Fe(1)–N(1)	2.149(7)	2.16(1)	O(3)···O(204)	2.97(2)	2.84(2)
Bond Angles					
	5·MeOH	7·MeOH	5·MeOH	7·MeOH	
X(1)–Fe(1)–O(1) ^b	160.1(3)	167.5(3)	X(1)–Fe(2)–O(3) ^b	171.3(2)	173.1(3)
X(1)–Fe(1)–O(2) ^b	89.0(3)	94.8(4)	X(1)–Fe(2)–O(102) ^b	91.7(2)	92.0(3)
X(1)–Fe(1)–O(101) ^b	87.3(2)	88.9(3)	X(1)–Fe(2)–O(202) ^b	93.3(2)	94.6(3)
X(1)–Fe(1)–O(201) ^b	93.3(2)	94.4(2)	X(1)–Fe(2)–N(3) ^b	98.7(3)	94.6(3)
X(1)–Fe(1)–N(1) ^b	97.7(2)	95.1(4)	O(3)–Fe(2)–O(102)	89.3(3)	90.0(4)
O(1)–Fe(1)–O(2)	110.3(4)	97.8(5)	O(3)–Fe(2)–O(202)	80.2(2)	79.2(4)
O(1)–Fe(1)–O(101)	73.7(3)	78.7(4)	O(3)–Fe(2)–N(3)	88.6(3)	90.2(4)
O(1)–Fe(1)–O(201)	83.8(3)	85.6(3)	O(102)–Fe(2)–O(202)	136.9(3)	133.7(4)
O(1)–Fe(1)–N(1)	88.8(3)	86.8(4)	O(102)–Fe(2)–N(3)	115.8(3)	119.7(4)
O(2)–Fe(1)–O(101)	174.5(3)	175.1(4)	O(202)–Fe(2)–N(3)	105.7(3)	105.4(4)
O(2)–Fe(1)–O(201)	86.3(4)	87.1(4)			
O(2)–Fe(1)–N(1)	84.8(3)	84.6(5)	Fe(1)–X(1)–Fe(2) ^b	101.2(2)	91.6(1)
O(101)–Fe(1)–O(201)	98.0(2)	95.9(4)			
O(101)–Fe(1)–N(1)	91.6(3)	91.8(5)			
O(201)–Fe(1)–N(1)	165.7(3)	167.9(5)			

^a Estimated standard deviations in the last significant figure are given in parentheses. See Figures 5, S1, S3, and S5 for atom-labeling schemes. ^b X = F in **5** and Cl in **7**. ^c Fe(1)–O(1A), 2.214(13), in **5**.

and O(11), at full occupancy and two (O)S–CF₃ moieties, O(12a), C(501a), F(1a)–F(3a) and O(12b), C(501b), F(1b)–F(3b), refined with isotropic thermal parameters at 0.75 and 0.25 occupancy, respectively. The triflate counterion in the lattice was disordered around a C₂-axis and thus refined as half occupied, except for O(14), which was shared by both positions and thus refined at full occupancy. The largest peak in the final Fourier map was 1.2 e⁻/Å³, located in the vicinity of the disordered CH₂Cl₂ molecule in the lattice.

[Fe₂(μ-Cl)(μ-XDK)(N-MeIm)₂(MeOH)₃](BF₄)·MeOH (7). Data were collected at 163 K with the ω–2θ scan technique. The positions of the Fe-, Cl-, N-, and O-atoms and all the non-hydrogen atoms of the N-methylimidazole were refined anisotropically. The phenyl ring of XDK was treated as a rigid group and refined isotropically. The largest peak in the final Fourier map was 0.78 e⁻/Å³, located in the vicinity of the MeOH molecule in the lattice.

[Fe(HXDK)₂(MeOH)₂ (8). Data were collected at 199 K with the ω–2θ scan technique. The positions of all non-hydrogen atoms were refined anisotropically. The largest peak in the final Fourier map was 0.37 e⁻/Å³ located in the vicinity of a methyl group of the xylene linker.

[Fe₂(μ-O₂CCH₃)(μ-XDK)(N-MeIm)₂(MeOH)₃](BF₄) (9). Data were collected at 199 K with the ω–2θ scan technique between 3° < 2θ < 33°. Because of the small number of unique reflections available, only the Fe atoms were refined anisotropically. All the other atoms were refined with isotropic temperature factors. The results revealed the chemical nature of the product.

[Fe₂(μ-O₂CC(CH₃)₃)(μ-PXDK)(N-MeIm)₂(O₂CC(CH₃)₃)]·C₅H₁₂ (4·C₅H₁₂). Data were collected at 193 K. The crystal quality was found to be acceptable on the basis of initial unit cell matrices and reflection profiles. The positions the Fe-, N-, and O-atoms were refined anisotropically. The three methyl groups of the bridging pivalate ion were rotationally disordered and modeled with two sets of three C-atoms, C(18a), C(19a), C(20a) and C(18b), C(19b), C(20b), refined at half occupancy. A disordered pentane molecule in the lattice was modeled with one C-atom refined at half occupancy in two positions, C(404a) and C(404b). The largest peak in the final Fourier map was 0.58 e⁻/Å³, located close to the disordered *tert*-butyl group of the bridging pivalate.

Stopped-Flow Kinetics Experiments. Data were collected on a Canterbury SF-41 stopped-flow instrument equipped with a MG-6040 rapid scanning diode array spectrometer (Hi-Tech). The flow lines were

dried and made strictly anaerobic by flushing with THF solutions of sodium-benzophenone ketyl, as previously described.⁶⁵ The formation of intermediates was studied in THF under pseudo-first-order conditions with an excess of O₂. Concentrations of the iron(II) complexes were ~1.5 mM, and the dioxygen concentration at saturation was 10 mM.⁶⁶ Rate constants for the formation of (μ-peroxo)diiron(III) intermediates were derived from absorbance changes at 660 nm (for **3**) and at 670 nm (for **4**). Data were collected and analyzed with the IS-2 Rapid Kinetics software,⁶⁷ and global analyses were carried out with SPECFIT.⁶⁸

Mössbauer Spectroscopy. Mössbauer spectra of polycrystalline samples of **3** (75 mg), **6** (85 mg), **7** (75 mg), and **4** (80 mg) dispersed in BN powder and a frozen solution of **4** (120 mg in ~1 mL of THF) were obtained by using a conventional, constant acceleration spectrometer. The spectrum of the intermediate of the reaction of **4** with dioxygen was obtained on a sample prepared by rapid freezing of a THF solution (100 mg of **4** in ~1 mL) to which O₂ had previously been added at 195 K and which had been stirred at 195 K for ca. 2 h. The γ-ray source was ⁵⁷Co in a Rh matrix maintained at 300 K. Isomer shifts were referenced to iron metal at 300 K. Spectral parameters were determined by least-squares fitting of the experimental data to theoretically calculated spectra by assuming Lorentzian line shapes.

Magnetic Susceptibility Measurements. Variable temperature solid state magnetic susceptibility measurements of **3** (26 mg), **6** (45 mg), and **7** (53 mg) were made by using a Quantum Design MPMS SQUID susceptometer equipped with a 5.5 T magnet. Samples were loaded in a drybox in gel capsules and suspended in plastic straws. The susceptibilities of the capsule and the straw were measured at the same fields and temperatures for accurate correction of their contribution to the total measured susceptibility. Diamagnetic corrections of –577.47 × 10⁻⁶, –638.60 × 10⁻⁶, and –583.10 × 10⁻⁶ cm³ mol⁻¹ for **3**, **6**,

(65) Feig, A. L.; Becker, M.; Schindler, S.; van Eldik, R.; Lippard, S. J. *Inorg. Chem.* **1996**, *35*, 2590–2601.

(66) *Oxygen and Ozone*; Battino, R., Ed.; Pergamon Press: Oxford, U.K., 1981; Vol. 7.

(67) *IS-2: Rapid Kinetics Software Suite*; Hi-Tech Scientific Ltd.: Salisbury, England, 1994.

(68) *SPECFIT: A Program for Global Least-squares Fitting of Equilibrium and Kinetic Systems Using Factor Analysis and Marquardt Minimization*; Spectrum Software Associates: Chapel Hill, NC, 1996.

and **7**, respectively, were calculated from Pascal's constants^{69,70} and applied. A total of 46 data points were collected at 5000 G in the temperature range of 4–300 K. The dependence of the magnetization versus the applied field was measured to ensure that the fields selected for the variable temperature studies of **3**, **6**, and **7** were within the linear presaturation regime of the magnetization versus H/T curves for the two compounds. The molar magnetic susceptibility data were fit to the expression derived from the spin-only isotropic exchange Hamiltonian $H = -2JS_1 \cdot S_2$, where $S_1 = S_2 = 2$. This expression is given as the first term in eq 1, where $x = J/kT$, TIP is the temperature-

$$\chi_M = (1 - p) \frac{Ng^2 \mu_B^2}{kT} \frac{2e^{2x} + 10e^{6x} + 28e^{12x} + 60e^{20x}}{1 + 3e^{2x} + 5e^{6x} + 7e^{12x} + 9e^{20x}} + \text{TIP} + p \frac{4.375}{T} \quad (1)$$

independent paramagnetism, p the mole percentage of a paramagnetic impurity, and $4.375/T$ the expression for the susceptibility of an $S = 5/2$ impurity. For all three complexes **3**, **6**, and **7**, no significant amount of impurity was present, so the last term of eq 1 was omitted ($p = 0$). Least-squares fits were carried out by using the program Model2.⁷¹

Results and Discussion

Synthesis and Structural Characterization. [Fe₂(μ -XDK)-(μ -O₂CPh)(ImH)₂(O₂CPh)(MeOH)] (3**) and [Fe₂(μ -O₂CC(CH₃)₃)(μ -PXDK)(*N*-MeIm)₂(O₂CC(CH₃)₃)] (**4**). Models for the Reduced Cores of RNR R2 Protein and MMOH.** The dicarboxylate ligand *m*-xylylenediamine bis(Kemp's triacid)-imide, H₂XDK (Figure 2), facilitates the synthesis of homo- and heterodimetallic complexes with a variety of different metal ions.^{49,72,73} Isolation of the remarkable diiron(III) solvento complex [Fe₂O(μ -XDK)(MeOH)₅(H₂O)](NO₃)₂ showed that this dinucleating ligand provides kinetic stability to dimetallic complexes, which cannot be achieved with simple carboxylate ligands.⁴⁹ This enhanced stability enabled us to prepare several diiron(II) complexes containing the {Fe₂(μ -XDK)}²⁺ core and, depending upon the presence of other anionic species in solution, a variety of different third bridging ligands. The propyl derivative, *m*-xylylenediamine bis(propyl Kemp's triacid)imide, H₂PXDK (Figure 2), affords analogous complexes with enhanced solubility in organic solvents.

The complex [Fe₂(μ -XDK)(μ -O₂CPh)(ImH)₂(O₂CPh)(MeOH)] (**3**) was assembled in good yields by allowing [Fe(H₂O)₆](BF₄)₂, the deprotonated ligand XDK, imidazole (ImH), and tetramethylammonium benzoate to react in a 2:1:2:3 ratio in a mixture of CH₂Cl₂/MeOH. Excess benzoate increased the product yield. Crystallization occurred by layering with Et₂O a concentrated MeOH/CH₂Cl₂ solution of **3** (ca. 0.1 M). A total of four carboxylate groups, two nitrogen donor ligands, and a solvent molecule, MeOH, are coordinated to the diiron center in **3**. Except for the solvent, the ligand type and composition exactly match those in the reduced diiron cores of MMOH and the RNR R2 protein. Even though in **3** the carboxylate ligands are arranged in a different geometry, this complex represents a very close model for the electronic environment of the diiron cores in these enzymes. Only one other example of a carboxylate-rich diiron(II) complex with only a single monodentate N-donor ligand per iron center has been reported in the literature.⁴⁶

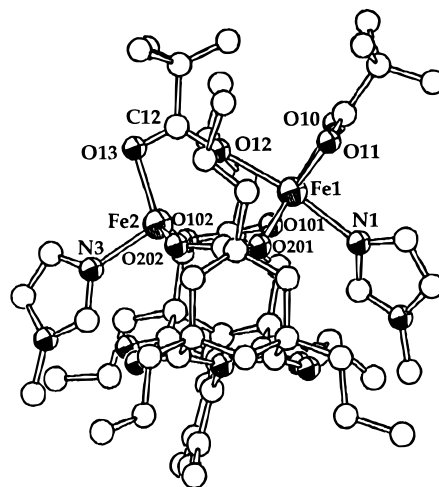


Figure 3. ORTEP plot of [Fe₂(μ -O₂CC(CH₃)₃)(μ -PXDK)(*N*-MeIm)₂(O₂CC(CH₃)₃)]·C₅H₁₂ (**4**·C₅H₁₂). For clarity, the hydrogen atoms are omitted and all the atoms are depicted as ideal spheres. An ORTEP plot showing the 50% probability thermal ellipsoids is given in Figure S8.

When *N*-MeIm or py was added as an N-donor ligand under the same reaction conditions used to prepare **3**, the analogous dinuclear complexes could not be obtained and the pentanuclear complexes [Fe₅(μ_3 -F)₂(μ -XDK)₂(L)₄(O₂CPh)₄], where L = *N*-MeIm or py, were isolated instead.⁷⁴ Reactivity studies with **3** were limited by its sparing solubility in organic solvents (MeOH, CH₃CN, and THF). Thus, we employed the more soluble H₂PXDK and pivalate carboxylate ligands to prepare the analogous tris(carboxylate-bridged) complex [Fe₂(μ -O₂CC(CH₃)₃)(μ -PXDK)(*N*-MeIm)₂(O₂CC(CH₃)₃)] (**4**), which is indeed very soluble in most organic solvents.

The structures of **3** and **4** were determined by crystallographic chemical analysis (CCA); ORTEP drawings are given in Figures 3 and S2 and selected bond lengths and angles in Table 2. The two iron(II) ions in **4**, bridged by the two carboxylate groups of PXDK and by a pivalate anion, are 3.584(3) Å apart and have distinctive coordination environments. Octahedral geometry at Fe(1) is achieved by coordination of *N*-methylimidazole and a bidentate pivalate ligand. The other iron, Fe(2), has only one terminal ligand, an *N*-methylimidazole, and is thus only 4-coordinate. The inner core of **3** is analogous to that of **4**, with the two iron(II) ions, 3.609(4) Å apart, bridged by the two carboxylate groups of XDK and by a benzoate anion. The pseudotetrahedrally coordinated Fe(2) is further bound by an imidazole, whereas the terminal sites of 6-coordinate Fe(1) are filled by a monodentate benzoate anion, an imidazole, and a MeOH molecule. The methanol is hydrogen bonded to the terminal benzoate ligand, O(11)···O(1), 2.50(2) Å, a feature shared by terminal water and glutamate ligands in MMOH_{red}.⁸ Weak interactions between Fe(2) and O(12), separated by distances of 2.52(1) and 2.466(8) Å in **3** and **4**, respectively, distort the metal from tetrahedral geometry, opening of the O(102)–Fe(2)–O(202) angle to 138.5(5)° in **3** and to 134.3(3)° in **4**. The coordination mode of the bridging benzoate and pivalate anions, with nearly linear bond angles of Fe(1)–O(12)–C(18) = 178(1)° in **3** and Fe(1)–O(12)–C(16) = 175.3(9)° in **4**, is unusual. This geometry cannot be classified according to either of the two standard ways by which carboxylate ligands usually bind metal ions, that is, via the syn or anti lone pairs. Rather, these bridging carboxylates may be regarded as involved

(69) O'Connor, C. J. *Prog. Inorg. Chem.* **1982**, 29, 203–283.

(70) Carlin, R. L. *Magnetochemistry*; Springer-Verlag: New York, 1986.

(71) Vef, A. *Model2. Fit and Evaluation Program*; Institut für Anorganische und Analytische Chemie, Johannes-Gutenberg-Universität Mainz, Germany, 1989.

(72) Yun, J. W.; Tanase, T.; Pence, L. E.; Lippard, S. J. *J. Am. Chem. Soc.* **1995**, 117, 4407–4408.

(73) Tanase, T.; Yun, J. W.; Lippard, S. J. *Inorg. Chem.* **1996**, 35, 3585–3594.

(74) Herold, S.; Lippard, S. J. *Inorg. Chem.* **1997**, 36, 50–58.

in a carboxylate shift,⁷⁵ with a structure between the canonical syn-anti and syn-syn coordination modes. Comparison of the reduced and oxidized forms of the diiron cores in the R2 subunit of RNR and in MMOH reveals significant carboxylate shifts,^{8,76,77} which presumably occur to open coordination sites or to allow conformational changes required during the catalytic reaction cycles.⁷⁵ The relatively short Fe...Fe distances in **3** and **4**, 3.609(4) and 3.584(3) Å, respectively, reveal that such shifts can occur in a concerted manner and do not require a significant increase in metal-metal distance. One other example of a molecule that displays a similar carboxylate coordination mode is the trinuclear complex [CaZn₂(crot)₆(6-MeQ)₂],⁷⁸ in which a bridging crotonate ligand links a tetrahedrally coordinated Zn(II) to the central octahedral Ca(II) ion, the Ca-O-C angle being 170.0(2)°.⁷⁹

Other Diiron(II) Complexes. Attempts to prepare a hydroxide-bridged diiron(II) complex by reacting [Fe(H₂O)₆](BF₄)₂, the deprotonated ligand XDK, and *N*-methylimidazole in the presence of 1 equiv of base, Et₃N or Me₄NOH, yielded instead the fluoride-bridged complex [Fe₂(μ-F)(μ-XDK)(*N*-MeIm)₂(MeOH)_{2.5}(H₂O)_{0.5}](BF₄) (**5**). The bridging fluoride ion originated from the tetrafluoroborate ion. Fluoride abstraction from BF₄⁻ readily occurs in the presence of base, which stabilizes the resulting BF₃ moiety, and has often been used as a synthetic tool to prepare transition metal fluoride complexes.^{80,81} In the presence of added Et₄NCl, the isostructural chloride-bridged complex [Fe₂(μ-Cl)(μ-XDK)(*N*-MeIm)₂(MeOH)₃](BF₄) (**7**) was assembled by following a similar procedure. When [Fe(H₂O)₆](OTf)₂ was used as the iron starting material, the triflate-bridged diiron(II) complex [Fe₂(μ-OTf)(μ-XDK)(*N*-MeIm)₃(MeOH)(H₂O)](OTf) (**6**) was isolated. A total of three *N*-MeIm ligands coordinate to the two iron centers in **6**, even though only 1 equiv per iron was available during the reaction.

The structures of **5**–**7**, determined by CCA, are presented in Figures 4, S3, S4, and S9. Selected bond lengths and angles for **5** and **7** are given in Table 3. The metal-metal distances reflect the nature of the ligands which, together with the two carboxylate residues of XDK, bridge the two iron(II) ions. In **5**, the small bridging fluoride ion gives rise to the shortest Fe...Fe distance in the series, 3.397(2) Å. The larger chloride ion in **6** forces the iron ions to be slightly further apart, Fe...Fe, 3.552(2) Å, whereas the largest Fe...Fe distance, 4.120(3) Å, occurs in the triflate-bridged complex **4**. Terminal ligation of the {Fe₂(μ-XDK)}²⁺ core in all three complexes is asymmetric, having both a 6- and a 5-coordinate center. In the isostructural fluoride- and chloride-bridged complexes **5** and **7**, an *N*-MeIm and two MeOH ligands complete the coordination sphere of one iron, Fe(1), and a second *N*-MeIm ligand and only one MeOH coordinate to the other, Fe(2). In the triflate-bridged complex **6**, two *N*-MeIm ligands and a water molecule are coordinated to Fe(1), whereas a third *N*-MeIm ligand and one MeOH complete the coordination sphere of Fe(2). In all three complexes, the solvent molecules coordinated on the same

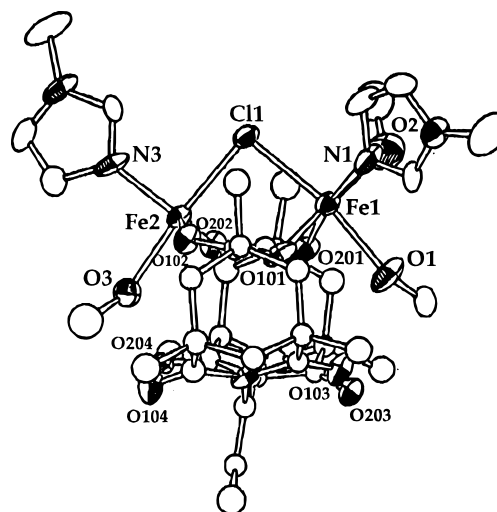


Figure 4. ORTEP plot of [Fe₂(μ-Cl)(μ-XDK)(*N*-MeIm)₂(MeOH)₃](BF₄)·MeOH (**7**·MeOH) showing the 50% probability thermal ellipsoids. For clarity, the hydrogen atoms are omitted.

side of the XDK ligand are hydrogen-bonded to carbonyl O-atoms of the XDK imide group, O(3)...O(204), 2.72(2) Å, in **5**, O(1)...O(103), 2.97(2) Å, and O(3)...O(204), 2.84(2) Å, in **7** and O(1)...O(103), 2.71(1) Å, and O(2)...O(204), 2.86(1) Å, in **6**. This feature is common among dinuclear XDK complexes and probably further stabilizes them.^{49,72,73}

As expected, the average Fe–O and Fe–N bond lengths for the 6-coordinate Fe(1) ions are generally longer than those for the 5-coordinate Fe(2) ion, (Fe(1)–N(1))_{av}, 2.154(6) Å, (Fe(2)–N(3))_{av}, 2.08(1) Å, (Fe(1)–O(CO₂⁻))_{av}, 2.12(5) Å, and (Fe(2)–O(CO₂⁻))_{av}, 1.97(1) Å. The bridging fluoride in **5** is bound slightly asymmetrically, being about 0.07 Å closer to Fe(2) than to Fe(1), Fe(1)–F(1), 2.230(5) Å, and Fe(2)–F(1), 2.166(4) Å. The bridging chloride binds the two iron ions more symmetrically, Fe(1)–Cl(1), 2.493(8) Å, and Fe(2)–Cl(1), 2.462(4) Å.

Reactions of [Fe₂(μ-Cl)(μ-XDK)(*N*-MeIm)₂(MeOH)₃](BF₄) (7**) with Thallium(I) Salts.** Mononuclear [Fe(HXDK)₂(MeOH)₂] (**8**). Attempts to substitute the chloride anion with biologically more relevant ligands by reacting [Fe₂(μ-Cl)(μ-XDK)(*N*-MeIm)₂(MeOH)₃](BF₄) (**7**) with different Tl⁺ salts was only partially successful. Reaction of **7** with 1 equiv of thallium(I) acetate in CH₂Cl₂/MeOH afforded a mixture of mononuclear [Fe(HXDK)₂(MeOH)₂] (**8**) and the tribridged complex [Fe₂(μ-O₂CCH₃)(μ-XDK)(*N*-MeIm)₂(MeOH)₃](BF₄) (**9**), as determined by CCA. Both **8** and **9** crystallized in colorless blocks, and it was very difficult to distinguish them from one another. Crystals of **8** have a slightly more regular shape. The X-ray analysis of **9** revealed that the two iron(II) ions are bridged by the three carboxylate groups of XDK and acetate, and that the terminal ligands are arranged in the same manner as in the fluoride- and the chloride-bridged complexes **5** and **6** (Figure S6).⁸² In the absence of other possible bridging ligands, reaction of **7** with 1 equiv of TlBF₄ again resulted in formation of mononuclear **8**.

The mononuclear compound [Fe(HXDK)₂(MeOH)₂] (**8**) precipitated readily as a white powder from the reaction of [Fe(H₂O)₆](BF₄)₂ with 2 equiv of H₂XDK in the presence of Et₃N in MeOH. Crystals suitable for CCA were obtained by layering a dilute MeOH solution of [Fe(H₂O)₆](BF₄)₂ and H₂XDK with a MeOH solution of Et₃N. Compound **8** also formed as an undesired side product during many of the reactions between

(75) Rardin, R. L.; Tolman, W. B.; Lippard, S. J. *New J. Chem.* **1991**, *15*, 417–430.

(76) Åberg, A. Thesis, Stockholm University, 1993.

(77) Nordlund, P.; Sjöberg, B.-M.; Eklund, H. *Nature* **1990**, *345*, 593–598.

(78) Abbreviations used: crot, MeCH=CHCO₂⁻; 6-MeQ, 6-methylquinoline; BIPhMe, bis(1-methylimidazol-2-yl)phenylmethoxymethane; TPA, tris(2-pyridylmethyl)amine; HPTP, *N,N,N',N'*-tetrakis(2-pyridylmethyl)-1,3-diamino-2-hydroxypropane, Et-HPTB, *N,N,N',N'*-tetrakis(*N*-ethyl-2-benzimidazolyl)methyl-1,3-diamino-2-hydroxypropane.

(79) Clegg, W.; Little, I. R.; Straughan, B. P. *Inorg. Chem.* **1988**, *27*, 1916–1923.

(80) Ten Hoedt, R. W. M.; Reedijk, J. *Inorg. Chim. Acta* **1981**, *51*, 23–27.

(81) Zang, Y.; Jang, H. G.; Chiu, Y.-M.; Hendrich, M. P.; Que, L., Jr. *Inorg. Chim. Acta* **1993**, *213*, 41–48.

(82) The unit cell parameters for **9** are *a* = 11.982(1) Å, *b* = 22.839(7) Å, *c* = 18.649(3) Å, and β = 91.56(1)°.

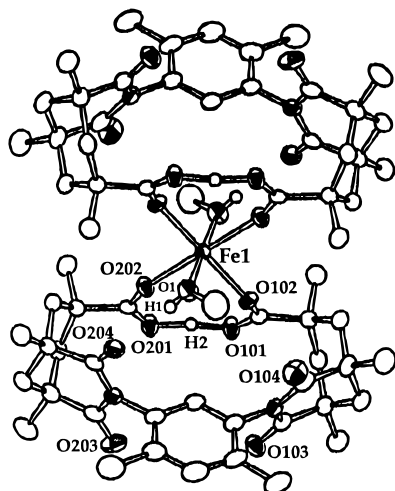
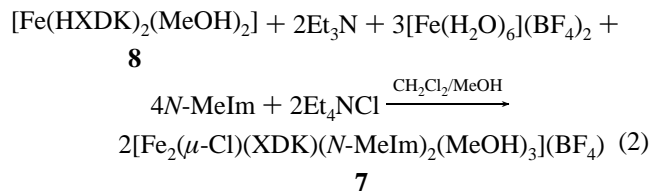


Figure 5. ORTEP plot of $[\text{Fe}(\text{HXDK})_2(\text{MeOH})_2]$ (**8**) showing the 50% probability thermal ellipsoids. For clarity, the hydrogen atoms are omitted. Selected interatomic distances (Å) and angles (deg): Fe(1)–O(1), 2.103(3); Fe(1)–O(102), 2.095(2); Fe(1)–O(202), 2.119(2); O(1)–Fe(1)–O(102), 92.7(1); O(1)–Fe(1)–O(202), 81.9(1); O(102)–Fe(1)–O(202), 94.24(9).

XDK and iron(II) salts, even in the presence of N-donor ligands, and precipitated out when these reactions were performed in MeOH. To avoid the formation of **8** in the Fe(II)/XDK system, a mixture of CH_2Cl_2 and MeOH was usually employed as solvent. This strategy allowed **8**, which is soluble in CH_2Cl_2 , to convert to the desired dinuclear compounds. For example, **8** afforded the dinuclear, chloride-bridged complex **7** following addition of 2 equiv of base and stoichiometric amounts of the other ligands, as shown in eq 2.



The X-ray structure of **8** revealed an octahedrally coordinated iron(II) ion bound, in equatorial positions, by four O-atoms of the carboxylate groups of two HXDK moieties and also by two axial MeOH ligands. An ORTEP plot of **8** is presented in Figure 5. This coordination mode for XDK is not unprecedented. The same arrangement occurs in the analogous Mg(II) complex $[\text{Mg}(\text{HXDK})_2(\text{H}_2\text{O})_2]$.⁸³ The asymmetric unit in the crystal consists of half of the molecule, with the iron atom located on an inversion center. The two monodentate carboxylate groups of HXDK bound to iron(II) are linked by a strong hydrogen-bond interaction between the noncoordinated O-atoms, O(101)···O(201), 2.438(4) Å, O(101)–H(2), 1.08(6) Å, O(201)···H(2), 1.37(8) Å. A further hydrogen-bond interaction is present between coordinated MeOH and a carbonyl O-atom of the diimide group of XDK, O(1)···O(204), 2.785(4) Å, O(1)–H(1), 0.73(4) Å, O(204)–H(1), 2.06(5) Å.

Magnetic Properties. Variable temperature magnetic susceptibility data for the three dinuclear compounds **3**, **6**, and **7** were obtained at 5000 G. Plots of the effective magnetic moment per molecule as a function of temperature in the 4–300 K range are given in Figure 6. The benzoate-bridged complex **3** has an effective magnetic moment per molecule (μ_{eff}), which slightly increases from $7.28 \mu_{\text{B}}$ at 300 K to $7.38 \mu_{\text{B}}$ at 50 K, whereupon there is a rapid decrease to $4.86 \mu_{\text{B}}$ at 4 K. The μ_{eff}

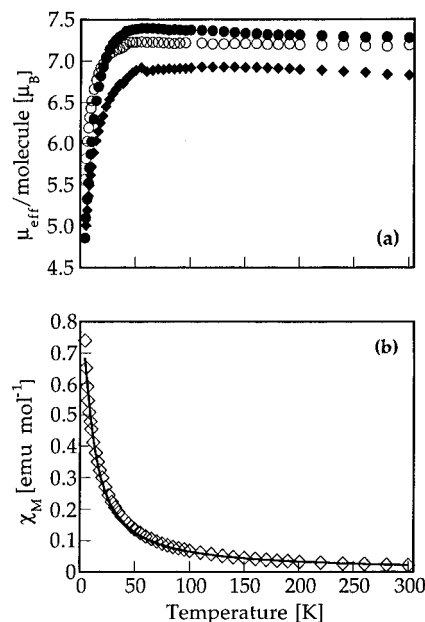


Figure 6. Effective moment (μ_{eff}) per molecule versus temperature (a) for $[\text{Fe}_2(\mu\text{-O}_2\text{CPh})(\mu\text{-XDK})(\text{ImH})_2(\text{O}_2\text{CPh})(\text{MeOH})]$ (**3**) (●), $[\text{Fe}_2(\mu\text{-OTf})(\mu\text{-XDK})(N\text{-MeIm})_3(\text{MeOH})(\text{H}_2\text{O})](\text{OTf})$ (**6**) (○), and $[\text{Fe}_2(\mu\text{-Cl})(\mu\text{-XDK})(N\text{-MeIm})_2(\text{MeOH})_3](\text{BF}_4)$ (**7**) (◆) and of the molar susceptibility (χ_{M}) versus temperature (b) for $[\text{Fe}_2(\mu\text{-O}_2\text{CPh})(\mu\text{-XDK})(\text{ImH})_2(\text{O}_2\text{CPh})(\text{MeOH})]$ (**3**). The solid line corresponds to the best fit, obtained by using the parameters described in Table S7.

values for the triflate-bridged complex **6** follow a similar trend. At 300 K, **6** has a μ_{eff} value of $7.19 \mu_{\text{B}}$ which increases to $7.23 \mu_{\text{B}}$ at 50 K, and then rapidly decreases to $5.57 \mu_{\text{B}}$ at 4 K. The μ_{eff} values for the chloride-bridged complex **7** are smaller than those for **3** and **6**, but vary analogously with the temperature. The μ_{eff} value slightly increases between 300 and 50 K, μ_{eff} (300 K) = $6.83 \mu_{\text{B}}$ and μ_{eff} (50 K) = $6.94 \mu_{\text{B}}$, and then rapidly drops to $5.01 \mu_{\text{B}}$ at 5 K. The μ_{eff} values for the three complexes **3**, **6**, and **7** at 300 K are close to the theoretical value of $7.62 \mu_{\text{B}}$ calculated from the spin-only equation for the effective moment of two independent $S = 2$ iron(II) ions with $g = 2.2$. The decrease of μ_{eff} at lower temperature indicates that the two high-spin iron(II) centers are weakly antiferromagnetically coupled. The molar magnetic susceptibility data were fit by using an expression derived from the spin-only Heisenberg Hamiltonian $\hat{H} = -2JS_1 \cdot S_2$, where $S_1 = S_2 = 2$. This simplified analysis does not take into account spin–orbit coupling and zero-field splitting, which may be relevant in the case of iron(II) ions.

The results of the best fits to the molar magnetic susceptibility (χ_{M}) data for **3**, **6**, and **7** are shown in Figures 6, S9, and S10, respectively. The final parameter sets obtained from these fits are summarized in Table 4. No corrections for paramagnetic impurities or temperature independent paramagnetism (TIP) were applied. For all three complexes a very small negative value was obtained for J , indicating that the two iron(II) ions are very weakly antiferromagnetically coupled and that the nature of the non-XDK bridging ligand does not have a substantial influence on the magnitude of the coupling constant. The small J values obtained from these fits suggest that, for a more accurate description of the magnetic interactions between the iron(II) ions of these complexes, the zero-field splitting parameter, D , should be taken into account. Nevertheless, the data clearly indicate the presence of only very weak antiferromagnetic interactions.

The magnetic properties of carboxylate-bridged diiron(II) model complexes depend significantly on the nature of the

(83) Yun, J. W.; Tanase, T.; Lippard, S. J. *Inorg. Chem.*, in press.

Table 4. Mössbauer and Magnetic Parameters for [Fe₂(μ-O₂CPh)(μ-XDK)(ImH)₂(O₂CPh)(MeOH)] (**3**), [Fe₂(μ-OTf)(μ-XDK)(N-MeIm)₃(MeOH)(H₂O)](OTf) (**6**), [Fe₂(μ-Cl)(μ-XDK)(N-MeIm)₂(MeOH)₃](BF₄) (**7**), [Fe₂(μ-O₂CC(CH₃)₃)(μ-PXDK)(N-MeIm)₂(O₂CC(CH₃)₃)] (**4**), MMOH, and RNR

compd	δ (mm/s)	ΔE _Q (mm/s)	Γ _{1/2} (mm/s)	J (cm ⁻¹)	g	ref
3	1.35	3.04	0.17	-0.51(2) ^a	2.11(2) ^a	<i>b</i>
	1.12	2.83	0.17			
6	1.44	2.54	0.26	-0.31(1) ^a	2.08(2) ^a	<i>b</i>
	1.19	2.70	0.15			
7	1.28	2.51	0.17	-0.45(2) ^a	2.18(1) ^a	<i>b</i>
	1.20	3.03	0.13			
4	1.34	2.94	0.15			<i>b</i>
	1.15	3.17	0.15			
4 (THF)	1.36	3.02	0.15			<i>b</i>
	1.14	3.15	0.15			
MMOH	1.30 ^c	2.87 ^c				21
	1.30 ^d	3.14 ^d		0.3 ± 0.1 ^d		88–90
RNR	1.26	3.13		0.3(2) ^e		91, 92, 96
				-0.5 ± 0.1 ^f		

^a Values obtained by fitting the data with a simplified expression derived from the spin-only Heisenberg Hamiltonian $H = -2JS_1 \cdot S_2$, where $S_1 = S_2 = 2$. ^b This work. ^c Isolated from *Methylococcus capsulatus* (Bath). ^d Isolated from *M. trichosporium* OB3b. ^e Reference 91. ^f Reference 92.

bridging ligands. The reported J values range from $-13 \geq J \geq -26$ cm⁻¹ for hydroxo and alkoxo, carboxylate-bridged complexes,^{38,45,47} to positive values between 1 and 15 cm⁻¹ for two ferromagnetically coupled iron(II) ions in bisalkoxo and bishalide complexes.^{40,81,84} A very weak antiferromagnetic interaction, comparable to that found in the present {Fe₂(μ-XDK)}²⁺ complexes, occurs in the tris(carboxylate-bridged) complex [Fe₂(O₂CH)₄(BIPhMe)₂], $J = -0.16(1)$ cm⁻¹.³⁹ For biscarboxylate complexes the value of the antiferromagnetic exchange coupling constant is also very small, $J = -1.5$ cm⁻¹ in [Fe₂(O₂CCH₃)₂L₂](ClO₄)₂, where L = *N,N'*-dimethyl-*N,N'*-bis(2-pyridylmethyl)ethane-1,2-diamine,⁸⁵ $J = -1.7$ cm⁻¹ in [Fe₂L₂(H₂O)₂](ClO₄)₂, where L' = bis(2-pyridylmethyl)(2-methylbenzoate)amine,⁸⁶ and $J \approx -1$ cm⁻¹ in [Fe₂(O₂CCH₃)₂(TPA)₂](BPh₄)₂.⁴² A recent study of a series of structurally analogous tris(carboxylate-bridged) trinuclear iron(II) complexes revealed that the sign of the weak exchange coupling between adjacent iron(II) ions changes with small perturbations in geometry.⁸⁷

Weak ferromagnetic exchange coupling has been reported for reduced MMOH from *Methylosinus trichosporium* OB3b, $J = 0.3 \pm 0.1$ cm⁻¹.^{88–90} Magnetic susceptibility data of the reduced R2 component of RNR were fit to give a similar weak ferromagnetic exchange interaction, $J = 0.3(2)$ cm⁻¹.⁹¹ A more detailed MCD saturation-magnetization study, however, discerned that the two iron(II) ions were weakly antiferromagneti-

cally coupled, $J = -0.5 \pm 0.1$ cm⁻¹.⁹² In reduced Hr, the two iron(II) ions are antiferromagnetically coupled with $-12 \geq J \geq -38$ cm⁻¹, in agreement with the presence of a hydroxo bridge.⁹³

Mössbauer Spectroscopy. Zero-field Mössbauer spectra of polycrystalline samples of **3**, **6**, and **7** were collected at 4 K. Figures S11–S13 display the spectra and theoretical least-squares fits to the data, and the resulting parameters are summarized in Table 4. All three spectra show two overlapping doublets, with a 1:1 ratio of integrated absorption intensities of the two spectral subcomponents, reflecting the two inequivalent iron(II) centers in the dinuclear complexes. The values of the isomer shifts (δ) for the two doublets in the spectra of **3**, **6**, and **7** are within the range expected for high-spin iron(II) ions.⁹⁴ The quadrupole splitting parameters are significantly different for the two sites, reflecting their different coordination environments. We tentatively assign the smaller ΔE_Q values (2.83, 2.54, and 2.51 mm/s for **3**, **6**, and **7**, respectively) to the 6-coordinate Fe(1), which displays a more symmetric, octahedral coordination sphere compared to the inherently more asymmetric pentacoordinate center Fe(2) in **6** and **7**, and the distorted tetrahedral Fe(2) ion in **3**, which might afford larger ΔE_Q values (3.04, 2.70, and 3.03 mm/s for **3**, **6**, and **7**, respectively). Similar assignments have been made for other diiron(II) complexes having inequivalent 5- and 6-coordinate sites.^{39,95} The isomer shift and quadrupole splitting values are comparable to those obtained for the diiron(II) centers of MMO^{21,96} and RNR (Table 4).⁹⁶

Zero-field Mössbauer measurements on polycrystalline and frozen THF solution samples of **4** were made at 20 K to obtain more information about the stability of the dinuclear core in solution. Figure 7 shows the traces and the theoretical least-squares fits to the data, which resulted in an almost identical set of parameters (Table 4). These results indicate that the biscarboxylate XDK and PXDK groups are very good ligands not only for assembling a variety of diiron(II) complexes but also, with the contribution of a third bridging ligand, for stabilizing the labile {Fe₂(μ-XDK)}²⁺ core in solution.

Reactivity with O₂. The reactivity toward dioxygen of the diiron(II) complexes **3–7** was investigated at different temperatures and in different solvents. The two tris(carboxylate-bridged) complexes [Fe₂(μ-O₂CPh)(μ-XDK)(ImH)₂(O₂CPh)(MeOH)] (**3**) and [Fe₂(μ-O₂CC(CH₃)₃)(μ-PXDK)(N-MeIm)₂(O₂CC(CH₃)₃)] (**4**), which have the same type of ligands as those bound to the diiron center in the active site of MMOH, formed metastable intermediates when allowed to react with dioxygen at low temperature. Addition of O₂ at 195 K to a yellow THF solution of **3** rapidly caused a color change first to deep green and then, after ca. 30 s, to orange. Stopped-flow kinetic experiments revealed that the formation of a green intermediate coincided with the rapid buildup of a broad band centered near 660 nm. An intermediate with a similar absorption maximum has been detected in the course of the reaction of the reduced diiron core of MMOH with O₂, and has been assigned as a (μ-peroxo)diiron(III) complex (H_{peroxo}), on the basis of its UV-vis, resonance Raman, and Mössbauer spectroscopic parameters.^{20,21} The extinction coefficient obtained after 64 ms, when

(84) Hendrich, M. P.; Day, E. P.; Wang, C.-P.; Synder, B. S.; Holm, R. H.; Münck, E. *Inorg. Chem.* **1994**, *33*, 2848–2856.

(85) Hazell, R.; Jensen, K. B.; McKenzie, C. J.; Toftlund, H. *J. Chem. Soc., Dalton Trans.* **1995**, 707–717.

(86) Hemmert, C.; Verelst, M.; Tuchagues, J.-P. *J. Chem. Soc., Chem. Commun.* **1996**, 617–618.

(87) Goldberg, D. P.; Telser, J.; Bastos, C. M.; Lippard, S. J. *Inorg. Chem.* **1995**, *34*, 3011–3024.

(88) Pulver, S.; Froland, W. A.; Fox, B. G.; Lipscomb, J. D.; Solomon, E. I. *J. Am. Chem. Soc.* **1993**, *115*, 12409–12422.

(89) Hendrich, M. P.; Münck, E.; Fox, B. G.; Lipscomb, J. D. *J. Am. Chem. Soc.* **1990**, *112*, 5861–5865.

(90) Fox, B. G.; Surerus, K. K.; Münck, E.; Lipscomb, J. D. *J. Biol. Chem.* **1988**, *263*, 10553–10556.

(91) Atta, M.; Scheer, C.; Fries, P. H.; Fontecave, M.; Latour, J.-M. *Angew. Chem., Int. Ed. Engl.* **1992**, *31*, 1513–1515.

(92) Coates Pulver, S.; Tong, W. H.; Bollinger, J. M.; Stubbe, J.; Solomon, E. I. *J. Am. Chem. Soc.* **1995**, *117*, 12664–12678.

(93) Reem, R. C.; Solomon, E. I. *J. Am. Chem. Soc.* **1987**, *109*, 1216–1226.

(94) Dickson, D. P. E.; Berry, F. J. *Mössbauer Spectroscopy*; Cambridge University Press: Cambridge, U.K., 1986.

(95) Rardin, R. L.; Bino, A.; Poganiuch, P.; Tolman, W. B.; Liu, S.; Lippard, S. J. *Angew. Chem., Int. Ed. Engl.* **1990**, *29*, 812–814.

(96) Lynch, J. B.; Juarez-Garcia, C.; Münck, E.; Que, L., Jr. *J. Biol. Chem.* **1989**, *264*, 8091–8096.

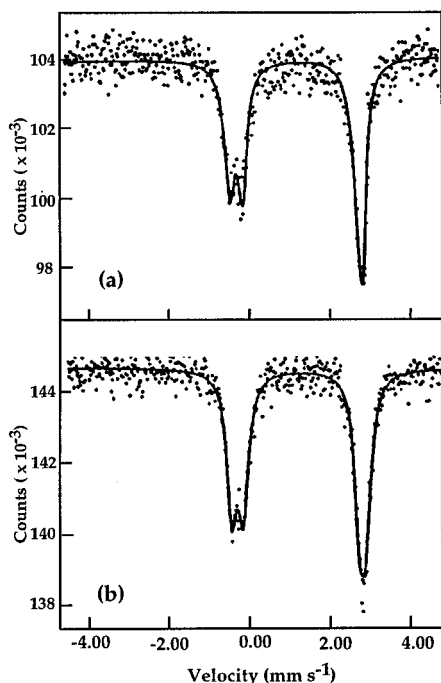


Figure 7. Mössbauer spectra at 20 K of (a) a polycrystalline and (b) a THF frozen solution sample of $[\text{Fe}_2(\mu\text{-O}_2\text{CC}(\text{CH}_3)_3)(\mu\text{-PXDK})(N\text{-MeIm})_2(\text{O}_2\text{CC}(\text{CH}_3)_3)]$ (**4**). The solid lines are the theoretical fits corresponding to the superposition of two inequivalent iron sites. See Table S5 for derived Mössbauer parameters.

the concentration of the green intermediate reached a maximum, was $\sim 170 \text{ M}^{-1} \text{ cm}^{-1}$ per diiron site. This value is about 1 order of magnitude smaller than expected for peroxo-to-iron charge-transfer bands found in other (μ -peroxo)diiron(III) model complexes ($\lambda_{\text{max}} = 580\text{--}700 \text{ nm}$, $\epsilon = 1300\text{--}3600 \text{ M}^{-1} \text{ cm}^{-1}$)^{22,23,25–27,45,47,97} and in H_{peroxo} ($\lambda_{\text{max}} \cong 600\text{--}650 \text{ nm}$, $\epsilon_{625} = 1500 \text{ M}^{-1} \text{ cm}^{-1}$).²⁰ The low value indicates that the present green (μ -peroxo)diiron(III) intermediate is never fully formed during the course of the reaction. Its decomposition must therefore occur at a higher rate than for the protein and possibly involves the bimolecular reaction between a diiron(II) and a (μ -peroxo)diiron(III) species, which occurs for other diiron(II) model complexes.^{1,65}

Figure 8 shows spectrophotometric changes observed every 4 ms up to 64 ms for the reaction of **3** with O_2 at 202.5 K. Kinetic studies carried out under pseudo-first-order conditions with excess dioxygen and monitored by time-dependent absorbance changes at 660 nm showed simple first-order buildup of the peroxide species. Rate constants ranging from 74 to 110 s^{-1} were obtained for a 1.63 mM THF solution of **3** at different temperatures between 202.5 and 213.2 K. An Eyring plot (Figure S14) of these preliminary data provided approximate values for the activation parameters, $\Delta H^\ddagger \approx 11 \text{ kJ mol}^{-1}$ and $\Delta S^\ddagger \approx -150 \text{ J mol}^{-1} \text{ K}^{-1}$. These values are in general accord with those obtained from detailed kinetic studies of the formation of the (μ -peroxo)diiron(III) complexes generated by reaction of $[\text{Fe}_2(\text{HPTP})(\text{O}_2\text{CPh})(\text{BPh}_4)_2]$ and $[\text{Fe}_2(\text{Et-HPTB})(\text{O}_2\text{CPh})(\text{BF}_4)_2]$ with an excess of O_2 in propionitrile.⁶⁵ Because the bridging XDK ligand is quite rigid, in order for a (μ -peroxo)diiron(III) intermediate to form, the bridging benzoate would have to change its coordination mode, possibly forming a chelate to Fe(2). Such a shift would not require a high activation energy, and would be facilitated by the interaction between Fe-

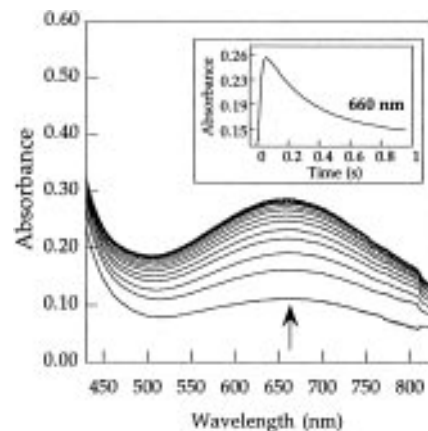


Figure 8. Spectral changes observed every 4 ms for a total of 64 ms in the reaction of $[\text{Fe}_2(\mu\text{-O}_2\text{CPh})(\mu\text{-XDK})(\text{ImH})_2(\text{O}_2\text{CPh})(\text{MeOH})]$ (1.63 mM) (**3**) with excess O_2 in THF at 202.5 K. The inset shows a kinetic trace at 660 nm for the first second of the reaction.

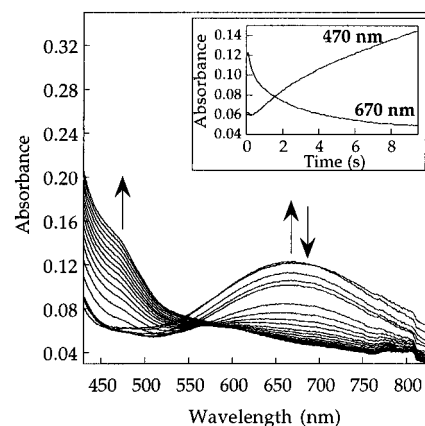


Figure 9. Spectral changes observed every 104 ms for five traces and every 730 ms for a total of about 10 s in the reaction of $[\text{Fe}_2(\mu\text{-O}_2\text{-CC}(\text{CH}_3)_3)(\mu\text{-PXDK})(N\text{-MeIm})_2(\text{O}_2\text{CC}(\text{CH}_3)_3)]$ (1.63 mM) (**4**) with excess O_2 in THF at 197 K. The inset shows kinetic traces for the decay of the purple intermediate (670 nm) and the growth of the red species (470 nm) for the first 10 s of the reaction.

(2) and O(12) present in the reduced form. The negative ΔS^\ddagger value is consistent with an associative process, as expected for O_2 binding.

The kinetic trace recorded at 660 nm (Figure 8, inset) showed that the decay of the green intermediate followed higher-order kinetics, in agreement with a possible bimolecular decomposition process. The UV-vis spectrum of the orange product remained unchanged as long as the reaction mixture was kept at 195 K. The solution rapidly turned yellow-orange upon warming to room temperature and gave rise to a slightly different UV-vis spectrum with absorption bands at 548 and 468 nm, characteristic of the (μ -oxo)diiron(III) or (μ_3 -oxo)triiron units (Figure S15).^{34,98–100}

Similar intermediates were observed during the reaction of **4** with dioxygen at 195 K. Addition of O_2 to a colorless THF or CH_2Cl_2 solution of **4** caused the initial formation first of a deep purple intermediate with a broad absorption band near 670 nm, which rapidly converted to a red species with a band at 470 nm. Figure 9 shows spectrophotometric changes observed every 104 ms for the first five traces and then every 730 ms for a total of about 10 s for the reaction of **4** with excess O_2 in

(98) Gorun, S. M.; Papefthymiou, G. C.; Frankel, R. B.; Lippard, S. J. *J. Am. Chem. Soc.* **1987**, *109*, 4244–4255.

(99) Armstrong, W. H.; Roth, M. E.; J., L. S. *J. Am. Chem. Soc.* **1987**, *109*, 6318–6326.

(100) Gorun, S. M.; Lippard, S. J. *Inorg. Chem.* **1988**, *27*, 149–156.

(97) Kitajima, N.; Tamura, N.; Amagai, H.; Fukui, H.; Moro-oka, Y.; Mizutani, Y.; Kitagawa, T.; Mathur, R.; Heerwegh, K.; Reed, C. A.; Randall, C. R.; Que, L., Jr.; Tatsumi, K. *J. Am. Chem. Soc.* **1994**, *116*, 9071–9085.

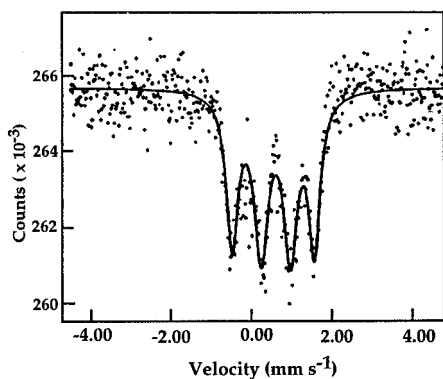


Figure 10. Mössbauer spectrum at 20 K of a THF frozen solution of the products of the reaction of $[\text{Fe}_2(\mu\text{-O}_2\text{CC}(\text{CH}_3)_3)(\mu\text{-PXDK})(N\text{-MeIm})_2(\text{O}_2\text{CC}(\text{CH}_3)_3)]$ (**4**) with O_2 at 195 K. The solid lines are the theoretical fits corresponding to the superposition of two inequivalent iron sites. See the text for derived Mössbauer parameters.

THF at 197 K. The pseudo-first-order rate constant for the formation of the presumed (μ -peroxo)diiron(III) intermediate, approximately 300 s^{-1} at 197 K, is larger than that obtained in the case of **3**. The decay of this intermediate and subsequent buildup of the red species, monitored by the time-dependent absorbance changes at 670 and 470 nm, respectively, followed higher-order kinetics (Figure 9, inset), again indicating possible aggregation processes. As observed for **3**, the red intermediate was stable at 195 K and decomposed to a yellow-green species with absorption bands characteristic of oxo-bridged polyiron(III) units upon warming to room temperature.

To obtain more insight into the nature of the red intermediate, a Mössbauer sample was prepared by adding dioxygen at 195 K to a THF solution of **4**, which was then frozen and measured at 20 K (Figure 10). Two doublets were observed having equal intensity and with similar isomer shifts, 0.53 and 0.59 mm/s, but very different quadrupole splitting, 2.03 and 0.73 mm/s, respectively. The values of the isomer shifts are within the range expected for high-spin iron(III) ions. The larger quadrupole splitting is in the range of values found for (μ -oxo)diiron(III) complexes,³⁴ whereas the second doublet might arise from a mononuclear iron(III) species. These preliminary data indicate that more than one species may be involved during the reaction of the tris(carboxylate-bridged) complexes **3** and **4** with dioxygen. More detailed rapid kinetic studies are currently in progress to probe further the mechanism of this reaction.

Complexes **5** and **7**, having a bridging fluoride or chloride ligand, were allowed to react with dioxygen at low temperature. No transient color changes were noted, although the originally colorless CH_2Cl_2 solution gradually turned yellow-orange, which typically signifies oxidation. This result may indicate that monoatomic bridging ligands in these complexes, in conjunction with the difficulty of XDK to undergo a carboxylate shift, make it difficult to form the (μ -peroxo)diiron(III) species. Reaction of these complexes with dioxygen may therefore involve intermolecular processes. For example, O_2 might be activated at the terminal, solvent-occupied sites of two different diiron(II) molecules. Addition of O_2 at 195 K to a colorless CH_2Cl_2 or THF solution of the triflate-bridged complex **6**, however, caused a color change to green. The buildup of this species, which was monitored by UV-vis spectroscopy, was complete after several hours. Absorption bands characteristic of (μ -oxo)diiron(III) and (μ_3 -oxo)triiron units were observed at 650, 450, 364, and 318 nm and became broader upon warming of the solution to room temperature (Figure S16). The weak intensity of the 650 nm absorption band excluded assignment as a (μ -peroxo)diiron(III) species. Preliminary stopped-flow experi-

ments showed higher-order kinetic behavior for the formation of this complex, monitored by time-dependent absorbance changes at 450 and 650 nm (Figure S16, inset). This result suggests that the green intermediate may correspond to one or more species resulting from aggregation processes.

Summary and Conclusions

Stable carboxylate-bridged diiron(II) complexes were prepared in good yield by using the dinucleating ligand XDK and its more soluble analogue PXDK. All the isolated complexes have a third bridging ligand, either chloride, fluoride, triflate, or another carboxylate anion. Two of the tris(carboxylate-bridged) complexes, $[\text{Fe}_2(\mu\text{-XDK})(\mu\text{-O}_2\text{CPh})(\text{ImH})_2(\text{O}_2\text{CPh})(\text{MeOH})]$ (**3**) and $[\text{Fe}_2(\mu\text{-O}_2\text{CC}(\text{CH}_3)_3)(\mu\text{-PXDK})(N\text{-MeIm})_2(\text{O}_2\text{CC}(\text{CH}_3)_3)]$ (**4**), are closely related to the reduced diiron cores in MMOH and RNR R2 protein. Their composition matches exactly the ligand types in the proteins, although arranged in a slightly different way, and thus reproduce the electronic environment of the two iron(II) ions. The X-ray structures of **3** and **4** revealed bridging benzoate and pivalate anions with an unusual coordination mode. The Fe–O–C bond angle is almost linear, and the O-atom interacts only weakly with the second iron center. The coordination mode of these bridging carboxylates is intermediate between the more common syn-anti and syn-syn modes and may facilitate further carboxylate shifting to allow for reaction with O_2 . Mössbauer spectra of polycrystalline and frozen THF solution samples were fit to almost identical parameters, indicating that the complexes stay assembled in solution. Stopped-flow studies of the reaction of **3** and **4** with dioxygen at low temperature revealed the rapid formation of colored intermediates, the first of which has an absorption maximum characteristic for peroxo-to-iron charge-transfer bands in (μ -peroxo)diiron(III) complex, analogous to what has been observed during the reaction cycle of MMO.

Acknowledgment. This work was supported by grants from the National Institute of General Medical Sciences and AKZO. S.H. thanks the Swiss National Science Foundation and the Jubiläums-Stiftung (Ciba-Geigy, Basel) for postdoctoral fellowships. We are grateful to Dr. G. P. Papaefthymiou for collecting and fitting the Mössbauer data and to A. M. Valentine for help with the stopped-flow experiments.

Supporting Information Available: Tables S1–S29, listing full crystallographic information, atomic coordinates and B_{eq} , anisotropic thermal parameters, and intramolecular bond distances and angles for **3–8**, and figures representing the numbering scheme for the XDK (Figure S1) and the PXDK (Figure S2) ligands, complete ORTEP plots of **3–7** and **9** (Figures S3–S8), plots of the molar susceptibility (χ_{M}) versus temperature, together with the best fits, for **6** and **7** (Figures S9 and S10), Mössbauer spectra at 4 K of polycrystalline samples of **3**, **6**, and **7** (Figures S11–S13), the Eyring plot for the reaction of **3** with O_2 (Figure S14), and the UV-vis spectra of the species obtained after addition of O_2 to **3** and **6** (Figures S15–S16) (83 pages). See any current masthead page for ordering and Internet access instructions.